A Comparison of Carlin-type Gold Deposits: Guizhou Province, Golden Triangle, Southwest China, and Northern Nevada, USA

JEAN S. Cline[a,*], John L. MUNTEAN[b], Xuexiang GU[c], Yong XIA[d]

[a]*University of Nevada Las Vegas, 4505 Maryland Parkway, Box 454010, Las Vegas, Nevada, USA*
[b]*Nevada Bureau of Mines and Geology and University of Nevada Reno, Reno, Nevada, USA*
[c]*School of Earth Sciences and Resources, China University of Geosciences(Beijing), Beijing 100083, China*
[d]*State Key Laboratory of Ore Deposit Geochemistry, Institute of Geochemistry, Chinese Academy of Sciences, Guiyang 550002, China*

Received 20 October 2012; accepted 2 November 2012

KEYWORDS
Geological comparison;
Carlin-type gold deposits;
Southwestern Guizhou;
Northern Nevada

Abstract Several Au deposits in Guizhou Province, southwest China, described as being similar to the highly productive Carlin-type gold deposits in northern Nevada, USA, were examined to identify similarities and differences between the two districts. Samples were collected along transects from low- to high-grade rock, where possible, and from stockpiles at the Shuiyindong, Zimudang, Taipingdong, Yata and Jinfeng (formerly Lannigou) deposits. Methods used to examine ore and alteration minerals included hand-sample description; reflectance spectroscopy using an ASD Terraspec spectrometer; analyses of hand samples by carbonate staining with Alizaren red and potassium ferricyanide; transmitted and reflected light petrography; chemical analyses, mineral identification, and imaging using a JEOL JSM-5610 scanning electron microscope; and quantitative chemical analyses using a JEOL JXA-8900 electron probe microanalyzer. Geochemical analyses of hand samples for 52 elements were done by ALS Chemex. Results indicate both similarities and differences between the two districts. Both districts have similar geologic histories, and deposits at both locations appear to have formed as a result of similar tectonic events, though the district in southwest China lacks evidence of coeval felsic igneous activity; however, the ore-stage minerals and the fluids that produced the minerals and deposits have some significant differences. The Nevada deposits were dominated by fluid-rock reaction in which host rock Fe was sulfidized to form Au-bearing pyrite. Although ore fluids sulfidized host rock Fe in the Guizhou deposits, the timing of Fe metasomatism is unknown, so whether the deposits formed in response to sulfidation or pyritization is unclear. Fluid-rock reaction between an acidic, aqueous fluid and highly reactive calcareous rocks in Nevada caused extensive decarbonatization of host rocks, jasperoid replacement of carbonate minerals, and alteration of silty rock components to illite and kaolinite. In Guizhou, CO_2-bearing ore fluids with temperatures and pressures approaching 100 ℃ and 500 bars greater than temperatures and pressures determined for ore fluids in the Nevada deposits, deposited Au-bearing pyrite. In examined Guizhou deposits these fluids carbonatized host rocks and formed both replacement and open-space-filling ore. The fluids, which may have been immiscible, were sufficiently overpressured to fracture wall rocks and to create significant open space filled by vein quartz. While deposit architecture, tectonic setting, and host rocks in Guizhou are quite similar to northern Nevada, ore and alteration minerals suggest that ore-forming processes in examined Guizhou deposits have important similarities to processes associated with formation of orogenic Au systems. The Guizhou deposits display characteristics of both Carlin-type and orogenic systems, perhaps indicating formation at conditions somewhat intermediate to conditions for Carlin-type deposits and orogenic systems.

1. Introduction

Although gold deposits similar to the Carlin-type gold deposits in northern Nevada have been identified in various parts of the world, no other region in the world contains trends or districts of deposits similar to those in Nevada (Hofstra and Cline, 2000; Cline et al., 2005). New discoveries have been periodically described as Carlin-type deposits, but to date these discoveries do not have grades or tons of ore comparable to the deposits in Nevada. Moreover, most of the discoveries outside of Nevada have been isolated occurrences. Clusters and trends of multiple deposits, such as the famous Carlin Trend, are hallmarks of the Nevada deposits. A possible exception is a cluster of deposits currently being mined in southwest China at the margin of the South China craton in a region called the Golden

* Corresponding author
E-mail address: jean.cline@unlv.edu

Triangle (Cunningham et al., 1988; Ashley et al., 1991: Ilchik et al., 2005; Peters et al., 2007; Su et al., 2009). This region is at the junction of the Yunnan, Guizhou and Guangxi Provinces and is also known as the Dian-Qian-Gui area (Fig. 1). These deposits exhibit many of the characteristics of the Nevada deposits including the presence of submicron Au in pyrite or marcasite, an association with As, Sb, Hg and Tl (Ashley et al., 1991; Hu et al., 2002; Peters et al., 2007), and a regional occurrence of multiple deposits. To date, however, the Chinese deposits are smaller on average than the Nevada deposits, especially in tonnage and contained gold. For example, Nevada has at least 13 deposits that contain more than 100 tonnes Au including at least one deposit that contains more than 1000 tonnes Au, whereas only the Jinfeng (Lannigou) deposit in the Golden Triangle has a reported resource of greater than 100 tonnes Au.

We visited several deposits in southwest China in order to compare and contrast them with the well-studied Nevada deposits, in an effort to understand the similarities and differences in the geologic processes that formed the two districts. Samples were collected from the Shuiyindong, Zimudang, Taipingdong, Yata and Jinfeng deposits, all located in southwest Guizhou Province (Fig. 1). Samples were collected along transects from low-to high-grade rock where possible, as well as from stockpiles. Such transects reduce variability owing to lithology changes; thus, observed changes in the rock can be more confidently related to mineralization and alteration processes. Transects were collected from drill core, underground mine drifts, and open pit benches that penetrated altered and mineralized carbonate and clastic rocks containing disseminated mineralization. We examined ore-stage and alteration minerals and compared their characteristics, along with features described in the literature, to the Nevada deposits.

Methods used to examine ore and alteration minerals included hand-sample description; reflectance spectroscopy using an ASD Terraspec spectrometer; analyses of hand samples by carbonate staining with Alizaren red and potassium ferricyanide; transmitted and reflected light petrography; chemical analyses, mineral identification, and imaging using a JEOL JSM-5610 scanning electron microscope; and quantitative chemical analyses using a JEOL JXA-8900 electron probe microanalyzer. Analyses of hand samples were done by ALS Chemex. For gold, a split of each sample was fired assayed with an atomic absorption finish, whereas the other split of each sample was treated with a near total four acid digestion, followed by a combination of ICP-AES and ICP-MS multi-element analyses and a mercury analysis using a hydride atomic absorption method.

2. Geology of the Nevada Carlin-type deposits

The geology of the deposits and districts in Nevada was described by Cline et al. (2005), and through district comparisons, key characteristics that define and are essential to the Nevada deposits were identified. Carlin-type gold deposits in Nevada are epigenetic hydrothermal replacement bodies that are mainly hosted by carbonate-bearing sedimentary rocks. They formed over a narrow time interval in the Late Eocene between 34 and 42 Ma (Tretbar et al., 2000; Hofstra et al., 1999) during a change from compression to extension (Henry, 2008). Over 80%–90% of the ounces in Nevada's Carlin-type deposits occur in four clusters of deposits. The largest is the Carlin Trend, followed by Cortez, Getchell, and Jerritt Canyon. The characteristics of the deposits in these four clusters are remarkably similar. The gold occurs mainly as structurally bound

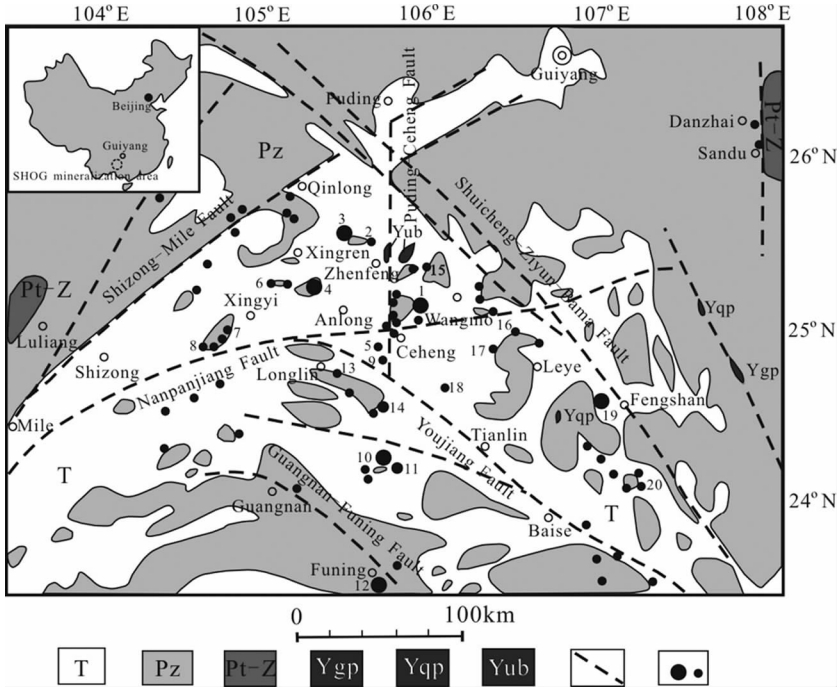

Figure 1 Simplified geologic map showing sediment-hosted disseminated gold deposit (SHGD) distribution in the Yunnan–Guizhou–Guangxi Triangle district (modified from Su, 2002).

T – Triassic strata; Pz – Paleozoic strata; Pt-Z – Proterozoic to Sinian strata; Ygp – Late Yanshannian granite porphyry; Yqp – Late Yanshannian quartz porphyry; Yub – Late Yanshannian ultrabasic rock; SHGD – sediment-hosted gold deposit: 1 – Jinfeng (formerly Lannigou); 2 – Shuiyindong; 3 – Zimudang; 4 – Getang; 5 – Yata; 6 – Nibao; 7 – Xiongwu; 8 – Lubuge; 9 – Banqi; 10 – Gaolong; 11 – Badu; 12 – Gedang; 13 – Maxiong; 14 – Longhuo; 15 – Nage; 16 – Lekang; 17 – Langquan; 18 – Baidi; 19 – Jinya; 20 – Linbu.

Au^{+}, or more rarely sub-micron sized native gold within trace element-rich arsenian pyrite or marcasite (Wells and Mullins, 1973; Arehart et al., 1993; Simon et al., 1999; Cline, 2001; Reich et al., 2005) that formed by sulfidation of host rock Fe (Hofstra et al., 1991). Pyrite, jasperoid quartz, illite, and kaolinite formed by replacement of wall rocks during fluid-rock reaction, whereas late ore-stage fluids precipitated orpiment, fluorite, realgar and calcite in open spaces as temperatures declined (Hofstra and Cline 2000; Cline et al., 2005). The ore bodies exhibit both structural and stratigraphic controls; breccias, many of which are collapse features, are important in some systems. Geologic relationships, apatite fission track data, and pressure estimates from fluid inclusion data are consistent with deposit formation at depths of mainly less than 2 km (Cline et al., 2005). Isotopic studies have identified meteoric water in many deposits and, significantly, magmatic or metamorphic water in other deposits (Hofstra and Cline, 2000; Muntean et al., 2011). Ore and alteration minerals as well as fluid inclusion studies in all deposits are consistent with temperatures of formation below ~250 ℃, and the deposits do not grade laterally or vertically into higher temperature mineral assemblages. For example, no coeval porphyry or skarn mineralization has been documented in any of the four main clusters. This characteristic distinguishes true Carlin-type deposits from Carlin-like deposits, which have similar geology, but are spatially and temporally linked to porphyry intrusive centers with early skarn mineralization, and which typically do not occur within trends or clusters (Cline et al., 2005; Muntean et al., 2011). Examples of these include the Cove deposit in Nevada (Johnson, 2000; 2003), and the Barney's Canyon deposit in the Bingham porphyry district, Utah (Cunningham et al., 2004).

Particularly important features and processes related to the formation of Carlin-type deposits (Cline et al., 2005), which are examined in this study include: (1) deposit architecture, which involved passive margin formation of carbonaceous, impure silty limestones or calcareous mudstones followed by millions of years of structural preparation, (2) alteration processes that include decarbonatization and the removal of CO_2 from the rock, silicification in the form of jasperoid replacement of carbonate minerals, and argillization through alteration of silty rock components to form illite and kaolinite, and (3) sulfidation of host-rock Fe by ore fluids that fixed Au and associated trace metals in pyrite.

3. Geology of the Chinese Carlin-type deposits

The Carlin-type gold deposits of Guizhou Province in southwest China (Fig. 1) are located in faults and in anticlines or domes in variably carbonaceous limestones and calcareous clastic rocks of Late Permian to Triassic age that formed along the southwest margin of the Precambrian Yangtze craton (Cunningham et al., 1988; Ashley et al., 1991; Peters et al., 2007). Stratigraphically controlled mineralization is found on the flanks of anticlines and domes, especially where intersected by faults. Fault-controlled mineralization occurs in compressive shear zones along reverse faults on the flanks of anticlines or domes (Su et al, 2009). Published descriptions of wall rock alteration are similar to the Nevada deposits (decarbonatization, silicification, argillization, and sulfidation) (Su et al., 2009), emphasizing the similarity of the Guizhou deposits to the Nevada deposits.

The deposits that were visited and examined during this study are located within about 100 km of each other in Triassic rocks,

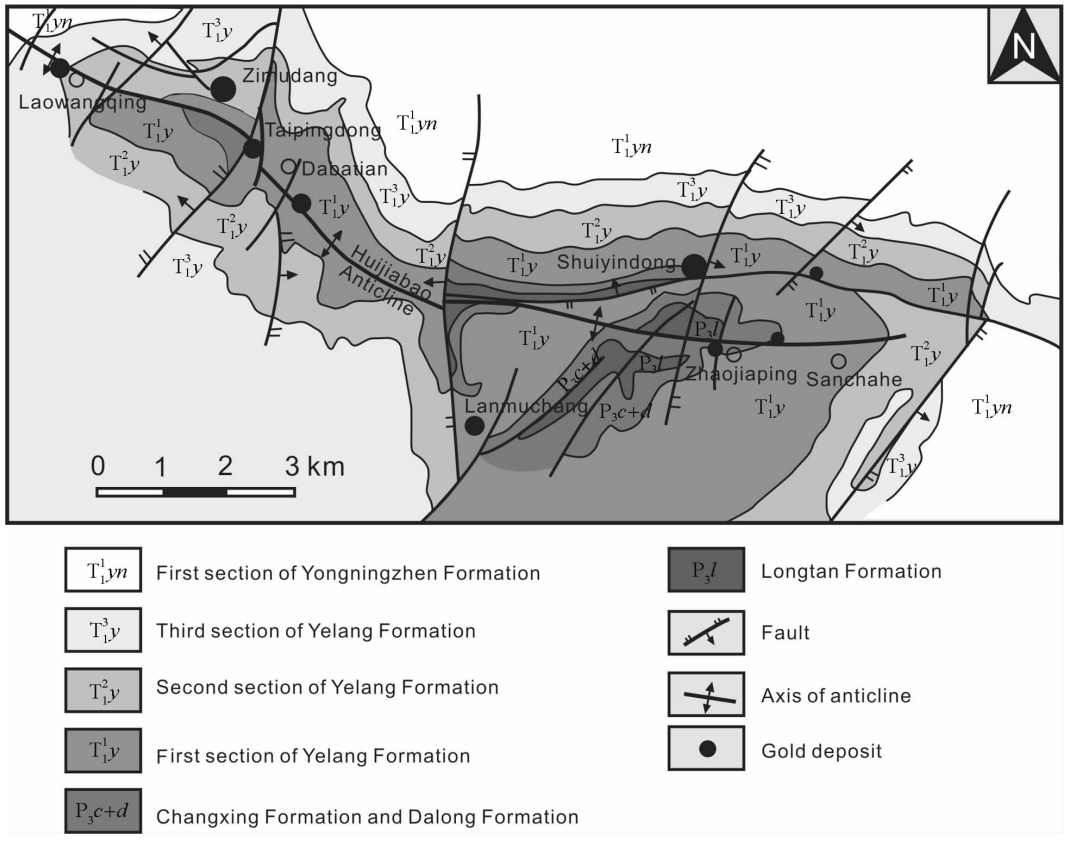

Figure 2 Map of the Huijiabao anticline showing the locations of the Zimudang, Taipingdong, and Shuiyindong deposits (after Guo, 1988).

within the Golden Triangle (Fig. 1). The geology of each deposit is briefly summarized below from the literature, and the samples collected and examined in this study are described.

3.1. *Shuiyindong*

The Shuiyindong deposit has proven gold reserves of 55 metric tonnes (t) Au (1.8 Moz) with average Au grades from 7 to 18 g/t (Xia, 2005). The mine produces about 400 000 t ore/yr and 2 tons Au/yr (~70 000 oz/yr) (Xia, 2005).

The following geology is summarized from Su et al. (2008; 2009). The Shuiyindong deposit lies on the eastern part of the Huijiabao anticline (Fig. 2), which is an east-trending symmetrical fold about 20 km long and 7 km wide with limbs that dip 10 to 20°. Deposit stratigraphy includes Middle Permian, Upper Permian, and Lower Triassic formations, which are largely bioclastic limestone, siltstone and argillite. Gold is preferentially disseminated in the bioclastic limestone and calcareous siltstone of the first and second units of the Upper Permian Longtan Formation at depths of 100 to 300 m (Fig. 3). Wall-rock alteration studies have identified dolomitization in addition to silicification and decarbonatization associated with Au. Arsenian pyrite forms rims on earlier pyrite, and is overgrown by arsenopyrite. Abundant Au-bearing pyrite and arsenopyrite are spatially associated with quartz, dolomite, and jasperoid. Electron probe microanalyses quantified Au and As in pyrite to 3800 ppm and 14 wt%, respectively, and quantified 300 – 1500 ppm Au in arsenopyrite.

Drill core samples examined in this study were collected along a transect from low-grade rock into ore in the inner of three gold horizons in the second (middle) member (unit P_3^2l) of the Upper

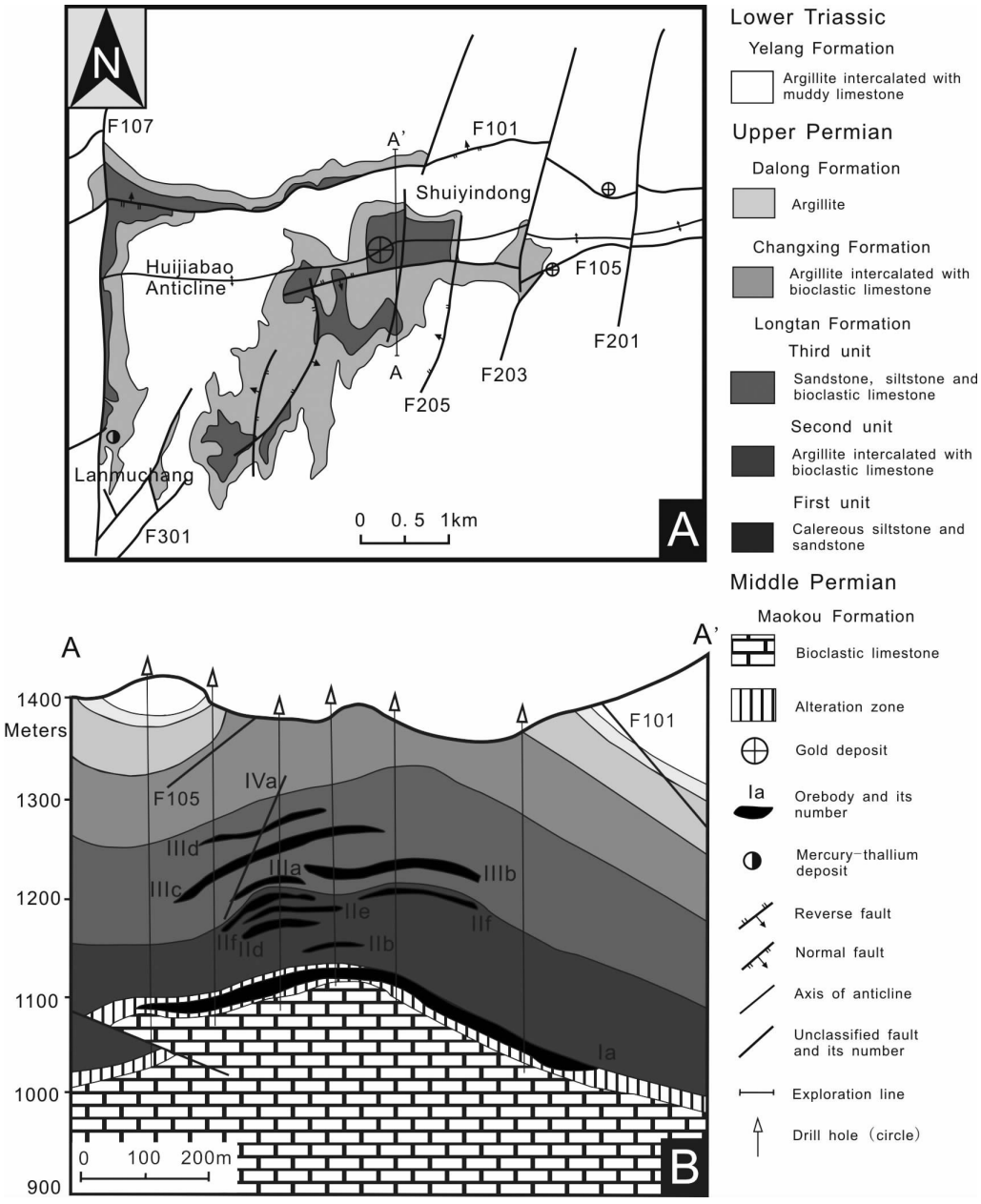

Figure 3 Simplified geologic map (A) and cross section (B) along A-A' exploration line of the Shuiyindong deposit (modified from Liu, 2001).

Permian Longtan Formation in ore body IIIC. This rock is described as argillite with interlayers of bioclastic limestone. Au is always in the bioclastic layers and the sampled ore layer is ~2.5 m thick. The highest grade sample (35.1 ppm Au, 726.3 m downhole) (Table 1) is from the middle of the high-grade zone. These rocks are medium-dark gray, competent, homogeneous in appearance, and moderately decalcified based on reaction to 10% HCl, though they lack the punky leached textures typically observed in decarbonatized zones in the Nevada deposits. Ore within the Shuiyindong deposit typically lacks fractures and open space, which likely explains the lack of realgar and stibnite in this deposit (Xia, unpublished data, 2011). Unmineralized rock below the ore zone is weakly altered mudstone, darker in color than the ore, has little to no reaction with 10% HCl, is moderately hard, and breaks perpendicular to the core yielding small disks of rock.

Table 1 Geochemical data for selected samples from the Carlin-type deposits in Guizhou

Elements		Samples											
		SH2	31116_726	31116_727	31116_730	37532_810	JF1	Yata1	Yata2	Yata3	ZUG1	ZUG6	ZUG11
Au	ppm	46.9	35.1	0.878	4.02	0.159	8.62	4.68	0.078	0.83	0.05	3.68	10.05
Ag	ppm	0.92	0.26	0.08	0.08	0.04	0.24	2.07	0.1	0.11	0.25	0.11	0.22
Al	%	3.15	0.48	7.72	1.37	0.11	1.18	1.39	0.27	0.44	5.86	2.86	5
As	ppm	2930	6470	4890	4270	37	689	855	>10 000	>10 000	2520	1395	4310
Ba	ppm	110	100	120	400	20	50	40	80	20	130	70	90
Be	ppm	0.7	0.27	1.59	0.58	0.57	0.21	0.27	<0.05	0.12	0.97	0.51	0.67
Bi	ppm	0.08	0.04	0.06	0.04	0.01	6.12	0.45	0.14	0.1	0.05	0.08	0.13
Ca	%	11.55	10.95	3.16	12.05	24	0.51	2.07	6.94	0.48	9.8	5.55	6.03
Ce	ppm	67.9	18.3	125.5	46.3	3.97	12.5	11.85	2.09	3.06	91.5	51.8	97
Co	ppm	16.3	4.7	52.5	7.2	0.7	2	36.2	0.7	0.8	23.4	13.9	23.2
Cr	ppm	185	25	314	23	6	15	19	4	8	59	31	46
Cs	ppm	2.86	0.54	15.05	1.53	0.13	0.84	1.53	1.18	0.58	5.69	2.08	4.16
Cu	ppm	19.5	57.5	64	13.5	1.9	10.5	60.2	2.7	5.5	72.2	40.7	96.9
Fe	%	6.84	3.33	8.49	5.98	1.01	0.9	4.81	0.56	0.72	6.06	3.58	5.9
Ga	ppm	10.75	2.41	22.8	5.31	0.35	2.81	3.23	0.5	1.07	17.45	9.53	17.7
Hg	ppm	13.8	12.5	14.2	6.1	0.23	>100	12.4	>100	4.74	6.5	8.35	13.7
K	%	0.91	0.14	2.58	0.42	0.04	0.46	0.54	0.06	0.15	1.74	0.88	1.59
La	ppm	33.7	11.1	55.8	24.9	3.4	6.6	6.2	1	1.5	43	25.7	45
Li	ppm	1.8	3.5	5.2	2.7	2.7	17.8	11.3	12.7	20	2.4	1.5	1.4
Mg	%	4.69	5.97	1.13	4.86	9.59	0.16	0.81	0.06	0.19	3.11	2.29	2.33
Mn	ppm	2980	2800	779	3110	807	103	465	438	169	1020	898	959
Mo	ppm	1.15	0.75	3.31	0.52	0.95	0.15	0.53	0.17	0.18	1.83	91.1	209
Na	%	0.09	0.04	0.06	0.02	0.05	0.02	0.01	<0.01	0.01	0.26	0.09	0.13
Nb	ppm	19.8	2	54.6	8.9	0.6	1.5	1.8	0.4	0.5	33	13.5	31.5
Ni	ppm	26.5	8.9	62.1	14.8	1.1	4.3	147	1.4	1.9	38.8	20	40.3
P	ppm	960	800	1480	1840	170	140	330	30	70	1600	1060	1290
Pb	ppm	3.5	4	7.5	2.4	0.5	44	66.1	0.7	2.1	4.9	7.2	10.5
Rb	ppm	30.6	6.6	107	16.9	1.8	17.8	21.5	2.4	6.7	61.2	32.9	60.9
S	%	2.99	2.7	7.83	1.24	0.28	0.81	4.49	0.66	0.97	1.49	2.36	4.66
Sb	ppm	36.6	35.6	32.2	16.8	0.5	3890	38.7	1230	185	23.1	44	91.2
Sn	ppm	2.1	0.6	2.9	0.9	<0.2	0.6	0.6	0.3	0.3	2.4	1.3	2.5
Sr	ppm	349	206	541	627	331	18.3	108.5	149	32.1	706	273	470
Ta	ppm	1.2	0.12	3.1	0.51	<0.05	0.1	0.14	<0.05	<0.05	2.22	0.86	1.97
Te	ppm	0.26	0.1	0.05	0.12	<0.05	0.11	0.1	1.24	0.1	<0.05	0.09	0.31
Th	ppm	3.7	0.7	7.3	2.1	0.2	2.7	2.5	0.3	0.5	6.5	3.5	6.5
Ti	%	0.446	0.042	1.915	0.226	0.009	0.064	0.068	0.009	0.015	1.25	0.497	1.115
Tl	ppm	6.77	20	16.25	6.83	0.19	0.76	0.83	3.27	0.11	0.71	9.68	14.6
U	ppm	3	0.5	1.9	1.1	0.4	0.6	0.6	0.2	0.1	1.4	1	1.4
V	ppm	178	48	334	51	10	14	22	2	5	167	82	145
W	ppm	17.1	2.8	26.7	5.2	0.3	0.9	3	0.5	0.5	7.9	13.3	24.2
Y	ppm	28.2	13.2	19.6	21.9	9.4	2.4	4.5	1.9	0.9	23.5	10.8	18.3
Zn	ppm	67	13	191	32	2	14	172	2	6	99	53	103
Zr	ppm	153	12.8	178.5	68.9	3.7	16.4	23.2	3.2	5	233	94.2	198

In this study we identified Shuiyindong sample 810m (159 ppb Au) as the least altered Guizhou sample examined based on geochemical assays (Table 1) and the presence of abundant calcite. This sample provides a basis for comparison in examining the degree and style of alteration of other samples from this and other deposits. Though minimally altered, the sample does contain 159 ppb Au, 37 ppm As, and 230 ppb Hg indicating reaction with ore fluids (Table 1). However, the sample also contains low Fe and Tl, and the highest Mg and Ca and lowest Hg, S, and Sb of the analyzed samples. Sample clasts, most of which are fossils or fossil fragments, react vigorously with 10% HCl and stain pink with Alizaren Red indicating they are comprised primarily of calcite (Fig. 4a). Fossil clasts also exhibit local, variable shades of blue where stained with potassium ferricyanide indicating variable Fe (Fig. 4b). Though most of the matrix between the clasts is sparry dolomite, the earliest matrix coating the clasts stained blue indicating the addition of Fe along fossil-matrix contacts. Minor fine-grained, high relief brassy pyrite is present in fossil clasts. Ca and Mg concentrations indicate an ~2－3∶1 dolomite to calcite ratio.

Moderately altered and mineralized Shuiyindong ore (sample 730 m) contains 4.02 ppm Au, 4270 ppm As, 6.1 ppm Hg, 6.83 ppm Tl, and 5.98 wt% Fe, indicating increased ore fluid reaction compared with sample 810 (Table 1). Drill core from this ore zone is competent and homogeneous, shows minor reaction with 10% HCl, and has a somewhat lower density than less altered rock, though decarbonatization textures typical of Nevada ore (Fig. 5a) are not observed. Small rounded pyrobitumen clasts were observed in rock clasts and matrix, but not in vein minerals. Carbonate staining indicates that calcite is not abundant and ferroan dolomite is of the predominant carbonate mineral.

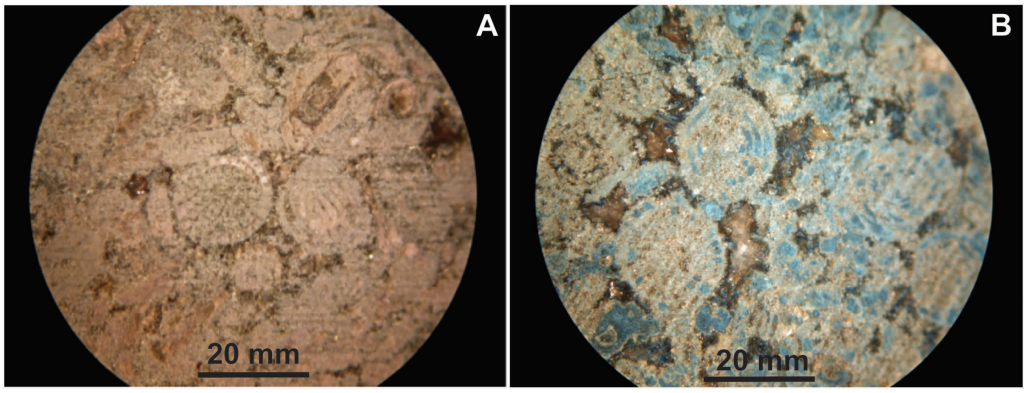

Figure 4 Photographs of minimally altered sample SH810 from the Shuiyindong deposit.
A－alizarin red stain indicates the presence of calcite; B－FeKCN stain in which blue indicates the presence of Fe.

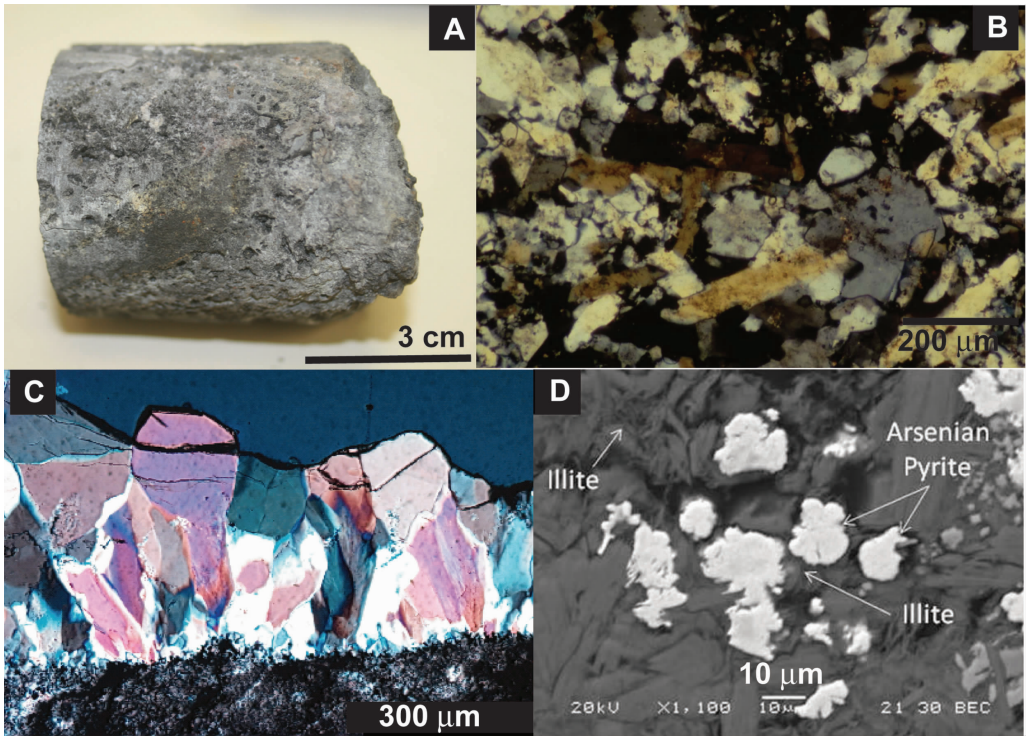

Figure 5 Alteration in Nevada deposits samples.
A－decarbonatized drill core, Getchell deposit, Nevada; B－transmitted cross-polarized light photomicrograph of jasperoid, Getchell deposit, Nevada; C－transmitted light photomicrograph of thick section of late-ore and post-ore drusy quartz on jasperoid, Betze-Post deposit, Nevada; D－BEI of illite intergrown with arsenian pyrite, Getchell deposit, Nevada.

In this section, narrow veins of quartz, carbonate, sulfide minerals, and open space cement fragmented bioclastic limestone. The fossils are both C-rich and C-free, suggesting variable introduction of petroleum that was later altered to pyrobitumen. Pyrite is both disseminated and in veins and correlates strongly with zones of dense pyrobitumen. Pyrite most commonly occurs as small rounded anhedral crystals or framboids that contain minor As. Some anhedral crystals and framboids have bright rims, visible under backscattered electron imaging (BEI), while others do not. The central areas and outer rims of crystals commonly contain 2 to 5 wt% and >5 wt% As, respectively. Arsenopyrite locally formed euhedral bladed crystals that replaced groundmass and formed overgrowths on pyrite. Arsenopyrite blades have rare rims visible under BEI that have elevated As: S ratios compared to arsenopyrite blades.

X-ray maps generated using the SEM (Fig. 6) show that regions containing Ca, Fe, and Mg carbonate minerals (Figs. 6d, 6e, and 6f) coincide with abundant sulfide minerals (Figs. 6a, 6b, 6e, and 6h). These regions also correspond with the presence of pyrobitumen. Comparison of the S and Fe maps shows that Fe is not restricted to sulfide minerals and much Fe is in carbonate minerals (Figs. 6b, 6d, 6e, and 6f) in the form of high Fe dolomite; stoichiometric dolomite is generally sparse. The high Fe carbonate-sulfide-pyrobitumen regions are rimmed by quartz, which has replaced original carbonate groundmass.

The highest grade sample from this ore zone (726 m, 35.1 ppm Au) is medium-dark gray in color and exhibits a minor reaction with 10% HCl. The sample was largely decalcified and has fine pore spaces, but lacks the visible decarbonatization texture characteristic of high-grade Nevada ore.

Fine pyrite, though abundant, is irregularly distributed and spatially associated with fossils and pyrobitumen. Coarser pyrite, alternatively, is more common in matrix cementing fossils and along contacts between fossils and matrix. All pyrites have high relief and are well polished and brassy in color. Rims are not visible under the microscope and only relatively rare coarse pyrites have rims that are visible under BEI (Figs. 7a, 7d, 7f). These rims can be complex from the coalescing of individual pyrite crystals during rim growth, or owing to the presence of multiple rims with variable compositions. Fine pyrites do not have rims that are visible under the microscope or under BEI; however, the centers of fine pyrites contain from below detection to ~ 7 wt% As, and the outer rim areas of these pyrites typically contain higher concentrations of As than pyrite centers. These observations suggest that the concentrations of trace metals increase gradually from the center of the crystals outward and that no discrete rim is present in these pyrites.

The carbonate rock matrix in sample 726 m was variably altered to quartz and local masses of illite. Fossil shells are both unaltered and composed of coarse calcite, and altered to fine, mottled intergrowths of high-and low-Fe dolomite, or to jasperoid. SEM analyses and maps (Figs. 8b, 8d, 8f) show that the abundant high Fe-dolomite that was dominant in moderately mineralized sample 730 is largely absent. Fossil matrix material is a fine-grained mixture of low-Fe dolomite, dolomite, Mn dolomite (Figs. 8b and 8d) or quartz (Fig. 8c). A coarse, well-zoned pyrite in matrix (Figs. 8b, 8d, 8f) is encompassed primarily by Fe-free or Fe-poor dolomite and a small patch of quartz (Fig. 8c). Patches of ferroan dolomite in high-grade rock have a consistent porous texture (Figs. 9f, 8a), whereas dolomite and Mn dolomite have a smooth, non-porous appearance (Fig. 9f). High-grade sample 726 m contains less Fe, but considerably more pyrite than low-to moderate-grade samples from this transect, consistent with sulfidation of Fe in ferroan dolomite to form ore-stage pyrite.

3.2. *Zimudang*

The Zimudang deposit, which occurs in Upper Permian and Lower Triassic Formations (Fig. 10), contains 60 t Au at a grade of 6 g/t (Hu et al., 2002; Peters et al, 2007). The deposit lies on the western limb of the Huijiabao anticline (Fig. 2) and contains structurally controlled mineralization that forms lens-shaped ore bodies within fracture and fault zones in altered rocks. The Lower Triassic Yelang Formation that contains the most favorable horizon in the mining area was deposited in a restricted tidal flat (Guo, 1988). The favorable horizon is comprised of thin-bedded to medium-bedded gray limestone and marl, with dolomite and calcareous siltstone interbeds. We sampled along a transect from low-to high-grade rock, in the middle part of the first section of the Yelang Formation. Samples were collected at one-meter intervals along the 1365 m level, from the hanging wall into the mineralized F_2 fault, a steep normal fault oriented sub-parallel to the axis of the anticline. The highest grade sample (ZUG11, 9.55 ppm Au) (Table 1) included rock from the fault zone and adjacent hanging wall.

Samples collected from the Zimudang deposit provide a pattern of alteration and mineralization similar to the patterns observed at Shuiyindong. Though sample ZUG1 contains the lowest concentration of Au in all assayed samples (50 ppb Au) it contains elevated concentrations of As, Fe, Cu, S, and Sb, along with lower concentrations of Ca and Mn than Shuiyindong sample 810 m, indicating it is significantly more altered. The sample, which displays undisturbed bedding, is comprised primarily of intergrown high-to low-Fe dolomite with lesser illite and minor quartz. Fossil shells that constitute a small percentage of the rock are altered to quartz, but have ferroan dolomite rims. The few small voids in the rock are rimmed by euhedral carbonate crystals. Local masses of dull gray-brown carbon are locally present.

Fine anhedral to subhedral pyrites and framboids (~0.5%) are disseminated throughout the rock matrix along with rare intergrowths of marcasite, sphalerite, and chalcopyrite. A dense accumulation of fine to coarse, anhedral to euhedral and framboidal pyrite forms a stratigraphic layer with pyrites increasingly disseminated in both directions away from this layer. Framboids and cores of fine pyrite crystals lack As. Minor As is indicated in the outer rim area of some fine pyrites, though no distinct rims are visible under the microscope or with BEI.

Sample ZUG11, the highest grade sample collected along this transect (9.55 ppm Au) was highly fractured and re-cemented primarily by quartz and pyrite. Quartz forms both narrow veins that cement broken rock fragments, and masses of jasperoid that replaced ferroan dolomite.

Disseminated and vein pyrite (~8%) is significantly more abundant compared to low-grade sample ZUG1, though both samples contain about 6% Fe. Masses of ore-stage pyrites are commonly associated with fine intergrowths of ferroan dolomite, which has a porous texture, and illite, along with minor local quartz. Fine pyrites contain As; coarse pyrite cores lack As, but the pyrites have complex rims with variable degrees of brightness under BEI imaging, and rims contain As, Au, and other trace elements in varying concentrations. As demonstrated at Shuiyindong, high-grade ore samples at Zimudang have

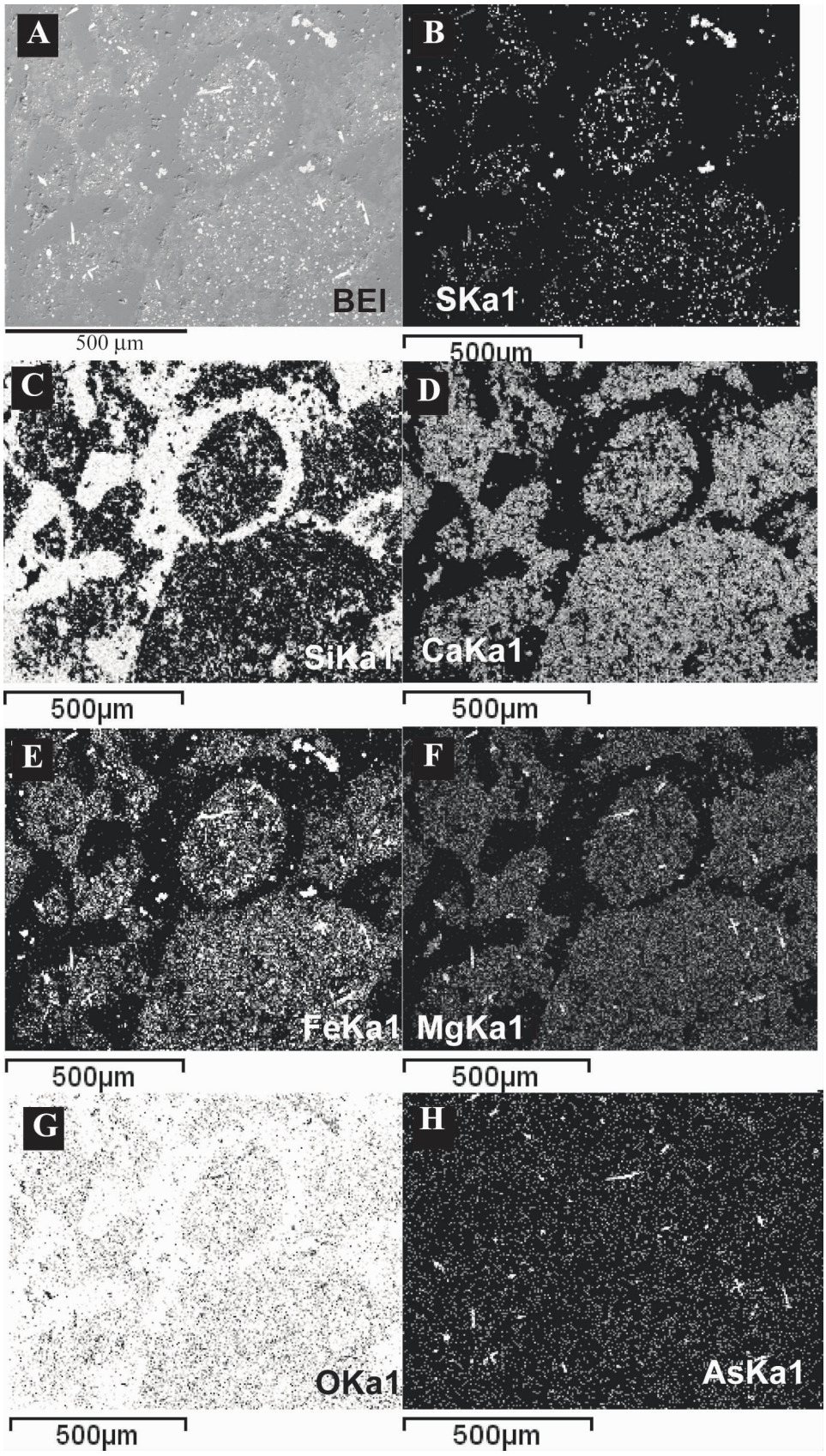

Figure 6 Backscattered electron image and elemental maps of moderate-grade alteration, Shuiyindong sample 730. Maps show that areas of carbonate minerals, dominated by ferroan dolomite, coincide with sulfide minerals and are rimmed by quartz. A – BEI; B – S map; C – Si map; D – Ca map; E – Fe map; F – Mg map; G – O map; H – As map.

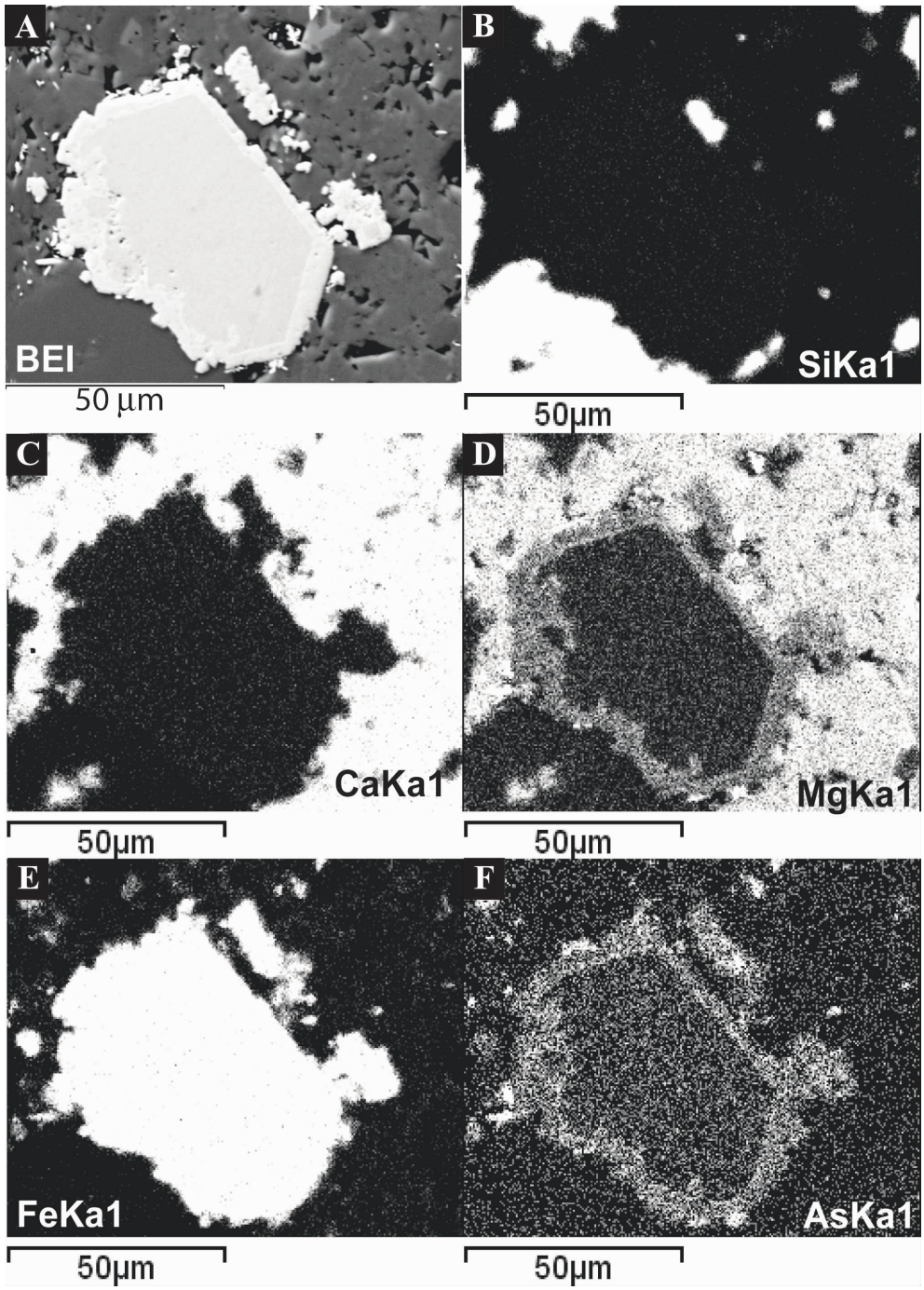

Figure 7 Backscattered electron image (A) and elemental maps (B－F) of high-grade alteration, Shuiyindong sample 726. Maps show a non-ore pyrite core with an ore-stage rim containing Fe (E), As (F), and Mg (D), in a matrix of dolomite (E, D) and lesser quartz (B).

increased pyrite at approximately constant Fe compared to lower-grade rock, indicating increased sulfidation of Fe in ferroan dolomite to form ore-stage pyrite.

3.3. *Yata*

Au in the Yata deposit, originally mined for As in realgar, was not recognized until the early 1980s (Tao et al., 1987). The deposit originally contained 15 tonnes of gold with a grade of 5 g/t. Gold is found in Member 2 of the Middle Triassic Xuman Formation, which is composed of fine-grained sandstone, siltstone, and mudstone (Ashley et al., 1991). Fault-controlled orebodies occur in altered calcareous and carbonaceous rocks along intersections of high-angle faults that cut the south limb of the east-trending Huangchang anticline and subsidiary folds (Zhang et al., 2003). Alteration includes decarbonatization, and formation of jasperoid quartz with reticulate textures, and formation of illite or illite-quartz veinlets associated with pyrite and arsenopyrite (Su et al., 2009). Late-ore stage mineralization is characterized by stibnite, orpiment, and realgar (Zhang et al., 2003).

Samples from the Yata deposit were collected from stockpiles

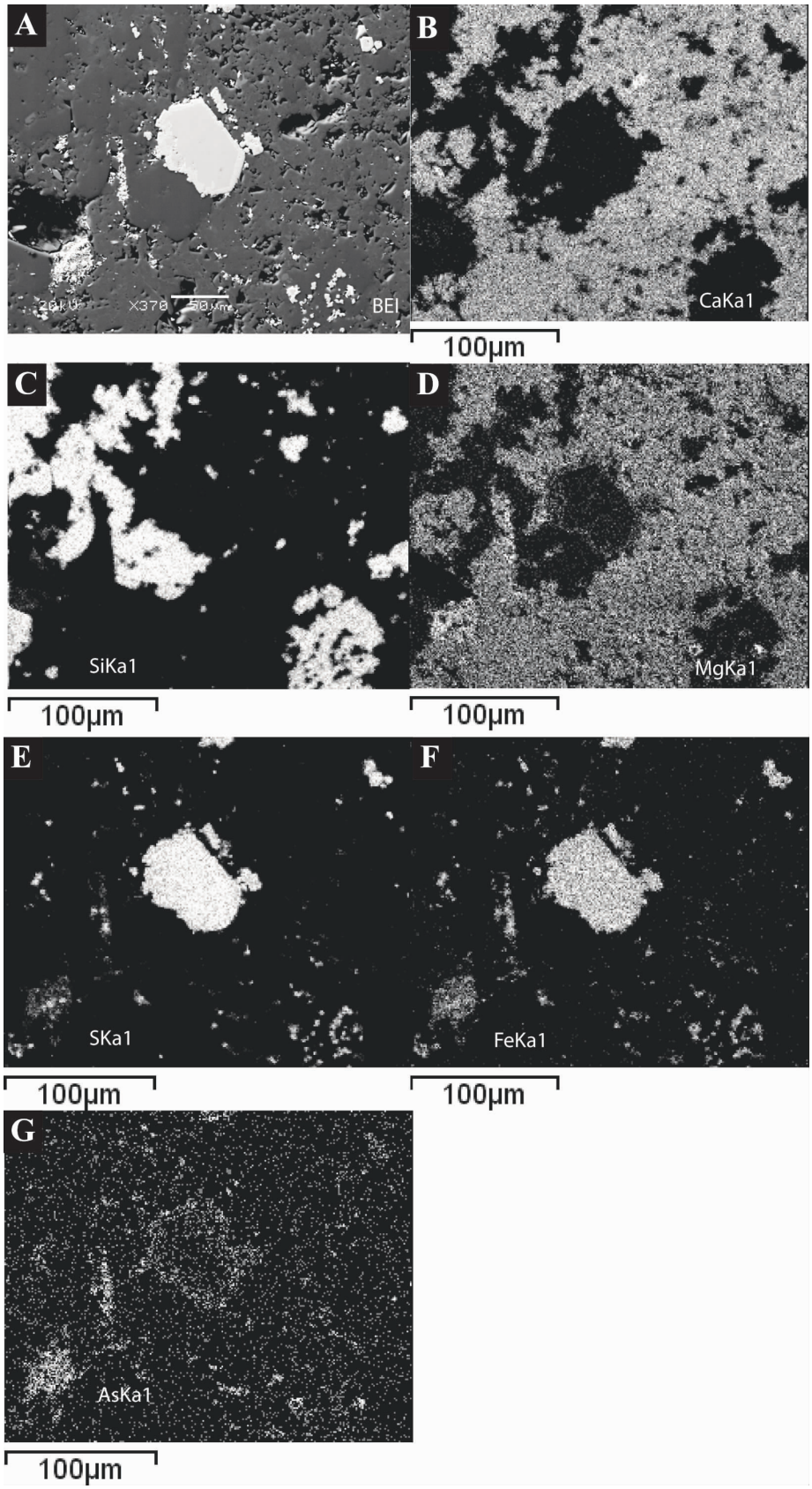

Figure 8 Backscattered electron image (A) and elemental maps (B－G) of coarse zoned pyrite crystal, high-grade Shuiyindong sample 726. BEI (A) shows the difference in the texture between smooth quartz and somewhat porous and essentially Fe-free dolomite.
A－BEI; B－Ca map; C－Si map; D－Mg map; E－S map; F－Fe map; G－As map.

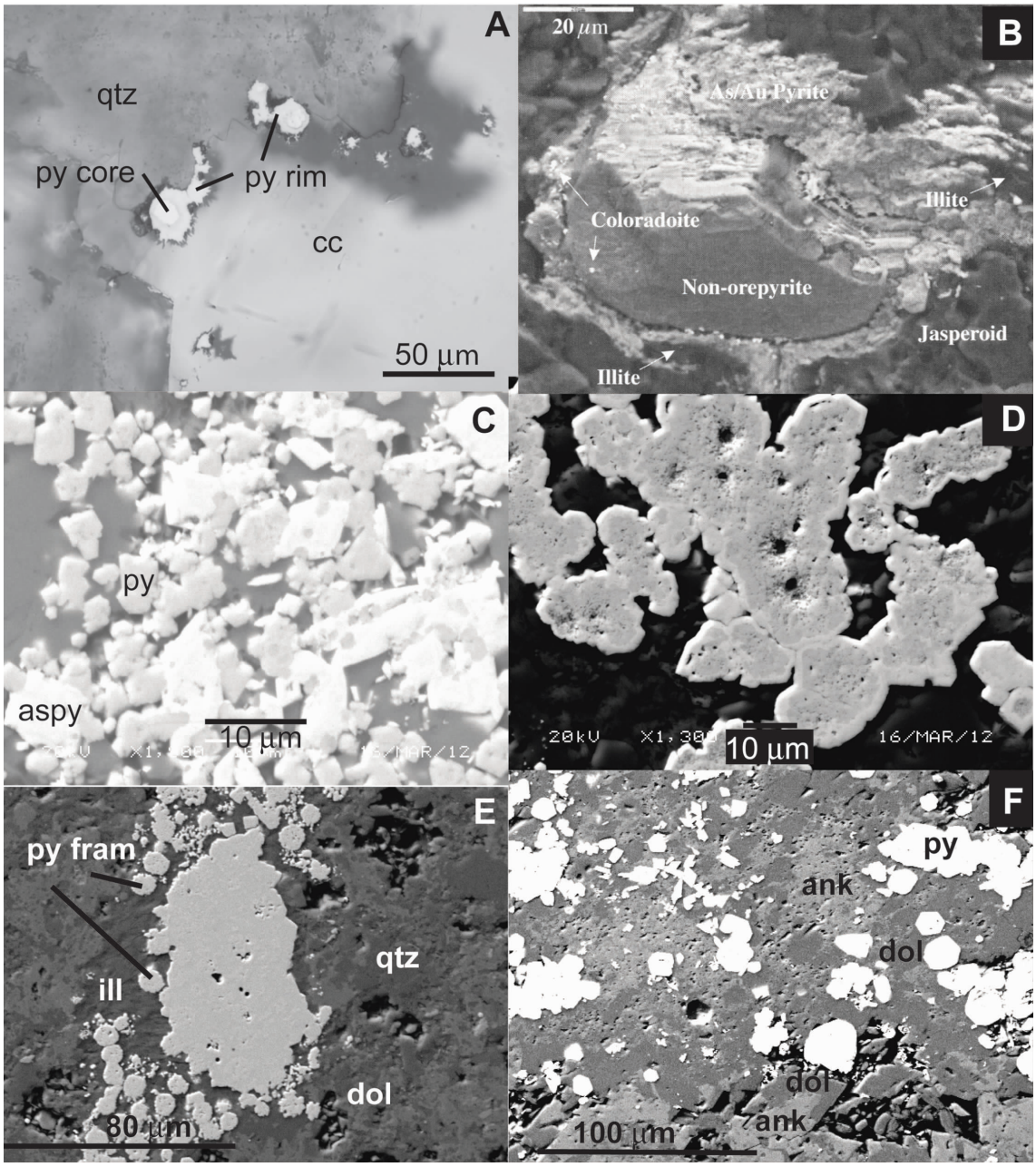

Figure 9 Photomicrographs and SEM images of pyrite in Nevada deposits and pyrite and arsenopyrite in the Guizhou deposits. A – reflected and transmitted plane polarized light image of ore-stage pyrite from the Getchell deposit, Nevada. B – BEI image of pre-ore pyrite core rimmed by ore-stage pyrite intergrown with illite and jasperoid, Turquoise Ridge deposit, Nevada. C – BEI image of fine-grained pyrite overgrown by brighter arsenopyrite from the Shuiyindong deposit, Guizhou, China. D – BEI image of coarse non-ore pyrite cores rimmed by ore-stage pyrite, Shuiyindong deposit, Guizhou, China. E – BEI of non-ore pyrite framboids in matrix of quartz, illite and dolomite, Zimudang deposit, Guizhou, China. F – BEI of fine-to moderately coarse-grained ore-and non ore-stage pyrite and arsenopyrite in a matrix of dolomite (dark and smooth texture) and ferroan dolomite (brighter and porous texture), Shuiyindong deposit, Guizhou, China.

and are comprised primarily of quartz, with lesser realgar, and stibnite. Quartz is dominated by fine-to very coarsely crystalline quartz vein material that cements minor angular fragments of wall rock. Wall rock fragments are dominantly fine-grained ferroan dolomite with carbonaceous material and lesser quartz, illite, and pyrite. Pyrite in the wall rock, ~5% to 7%, is fine (<10 – 75 μm), brassy, subhedral, high relief, has no visible rims, and is spatially associated with ferroan dolomite. Pyrite is most abundant along vein-wall rock contacts, consistent with precipitation in response to fluid-rock reaction.

Quartz veins contain minor stibnite, calcite, ferroan dolomite, realgar, and pyrite, and trace marcasite, chalcopyrite, and sphalerite. Vein quartz varies from fine anhedral to coarse euhedral crystals (~1 cm) and contains patches or vein-like zones of ferroan dolomite. Fine to coarser (<10 to >100 μm) pyrite, similar in character to pyrite in wall rock, is spatially associated with ferroan dolomite, especially along contacts with quartz. Euhedral quartz was overgrown by coarse botryoidal

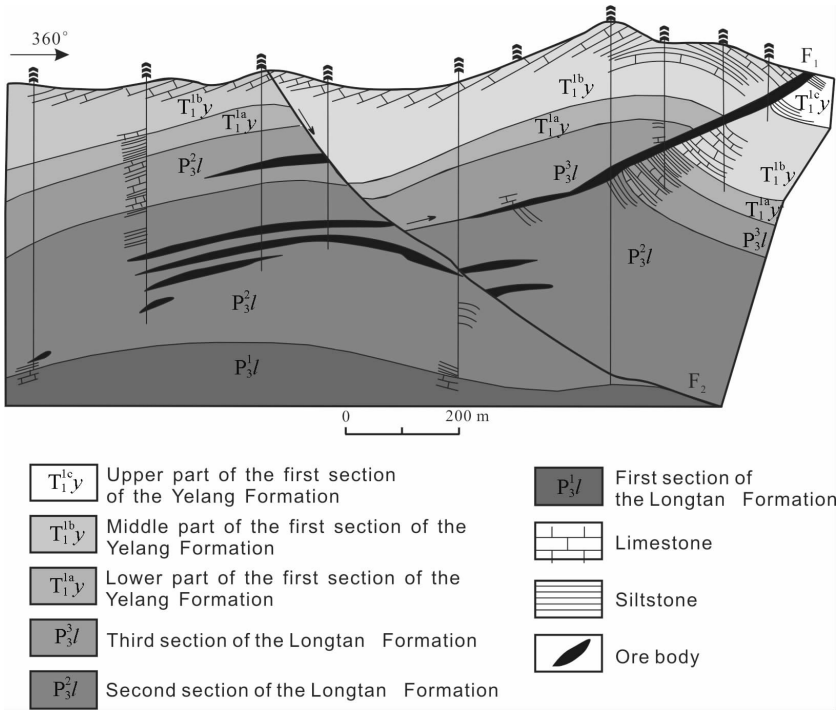

Figure 10 Map of the 32－32' exploration section of the Zimudang gold deposit (modified from Wang et al., 1994).

stibnite, which was in turn overgrown by coarse calcite. Realgar filled or partially filled remaining open space and forms overgrowths on earlier minerals (Fig. 11). Stibnite is locally intergrown with pyrite and rare marcasite, chalcopyrite and sphalerite.

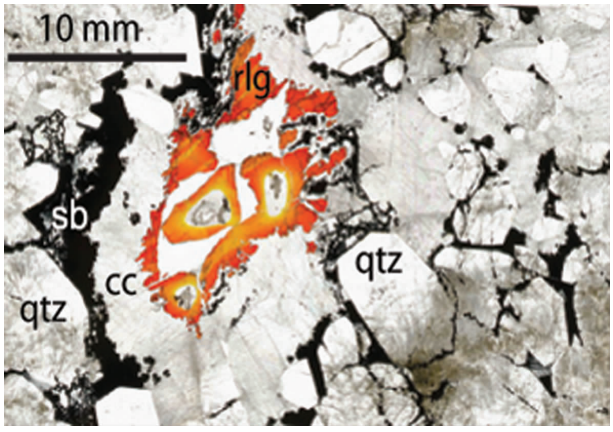

Figure 11 Polished section of late-ore stage mineralization from the Yata deposit showing overgrowth relationships from early to late: Euhedral quartz, stibnite, calcite, and realgar.

3.4. *Jinfeng (Lannigou)*

Jinfeng has reserves of 108.9 tonnes (3.5 million ounces) Au (Ilchik et al., 2005) with an average grade of 5.2 g/t and is estimated to contain at least a 164.85 tonnes (5.3 million ounce) Au resource at an average grade of 4.5 g/t, making it one of the largest known Au deposits in southwestern China (Chen et al., 2011). The ore is almost entirely fault-hosted and structurally controlled and very little ore is disseminated in the adjacent host rocks (Ilchik et al., 2005; Chen et al., 2011). According to Ilchik et al. (2005), gold occurs in carbonate-and clay-rich to fine-sand facies in turbidites in the mid-Triassic Bianyang and Xuman Formations that contain accessory carbonaceous material, diagenetic pyrite, and carbonate cement. A complex structural history indicates early extension followed by three periods of compression, and ore bodies take the form of structural ore fluid conduits (Ilchik et al., 2005). Au is in arsenian pyrite and, in lesser concentrations, in later arsenopyrite, both of which are followed by a late-ore stage containing realgar + orpiment + cinnabar and native As in calcite and lesser quartz.

Ore samples from Jinfeng, observed in this study, are similar to those from Yata in that they contain angular fragments of wall rock consisting of primarily quartz and illite with minor dark carbonaceous material, pyrite, and rutile. Wall rock fragments are cemented in a matrix of vein quartz that has euhedral crystals to 1 cm, with ~1% coarse-grained stibnite, lesser coarse-grained cinnabar, and minor realgar. Both stibnite and cinnabar conform to earlier euhedral quartz and realgar locally fills fractures. High relief, brassy pyrite is largely restricted to wall rock clasts and is fine-grained (<20 μm), though crystals reach 100 μm, and typically contain <3 wt% As. Wall rock fragments are cut by pre-breccia quartz veins and are rimmed by quartz crystals, indicating multiple fracturing events.

3.5. *Fluid Inclusion Studies*

Fluid inclusion studies reported in the literature for the Guizhou deposits have identified pre ore-, main ore-and late ore-stage fluids. Much quartz in the Guizhou deposits precipitated in open space, is considerably coarser than jasperoid that typifies the Nevada deposits, and contains fluid inclusions that reach 20 μm or larger (Su et al., 2009), significantly larger than inclusions observed in the Nevada deposits though much smaller inclusions (3 to 10 μm) have been examined in other studies (Hu et al., 2002). The data described below are from Su et al., 2009, for

the Shuiyindong and Yata deposits, and results are generally similar to data from other deposits in the region (Hu et al., 2002; Zhang et al., 2003; Gu et al., 2012). Pre main-ore stage barren, milky quartz veins contain two-phase, liquid-rich aqueous inclusions. Homogenization temperatures range from about 190 − 260 ℃ with a mode at ~230 ℃, and salinities vary from about 5 to 7 wt% NaCl equivalent. Microthermometry did not indicate the presence of CO_2, which is therefore <2.4 mol% (Bodnar et al., 1985); however, Raman spectroscopy detected peaks of CO_2, N_2, and CH_4. The trapped fluids are interpreted as part of the hydrothermal event that produced the Au mineralization, but they precipitated early barren vein quartz that predates deposition of the bulk of Au-and As-bearing pyrite; laser ablation induced coupled plasma mass spectrometry has quantified Au in two of these pre main-ore stage inclusions.

Main ore-stage fluids that precipitated vein quartz or jasperoid and the bulk of the Au-and As-bearing pyrite, form 2-or 3-phase H_2O-CO_2 inclusions. Two-phase inclusions generate a third phase on cooling. Final homogenization temperatures range from about 190 to 245 ℃ though many inclusions decrepitated prior to final homogenization. Salinities vary from about 1.6 to 3.3 wt% NaCl equivalent. Calculations determined that inclusion fluids contained from 6.3 to 8.4 mol% CO_2, and that these fluids were trapped at pressures from 450 to 1150 bars, corresponding to depths of 1.7 to 4.3 km assuming lithostatic pressure. Raman spectroscopy analyses confirmed the presence of moderate CO_2 as well as minor N_2 and trace CH_4. These inclusions, which were also found in late ore-stage minerals, were interpreted as possibly having trapped one fluid end member produced by unmixing of H_2O-CO_2 fluids, with the other end member fluid consisting of CO_2 trapped in late ore-stage minerals.

Late ore-stage fluids were trapped as abundant monophase CO_2 inclusions and rare two-phase CO_2-H_2O inclusions that contain 45 to 90 vol% CO_2. The CO_2-H_2O inclusions decrepitated on heating and no homogenization temperatures were obtained. Salinities varied from ~0 to 9 wt% NaCl equivalent. The CO_2-dominant fluids precipitated late-ore drusy quartz, realgar, stibnite and calcite. The monophase CO_2 inclusions, along with main-ore stage H_2O-CO_2 fluids are interpreted to represent immiscibility.

4. Comparison of the Nevada and Guizhou deposits

4.1. *Tectonic and Geologic Setting*

The tectonic and geologic setting for sedimentary rock-hosted gold deposits in southwest Guizhou Province (Zhang et al., 2003; Ilchik et al., 2005; Zaw et al., 2007; Peters et al., 2007; Li and Li, 2007; Su et al., 2009; Gu et al., 2012, Chen et al., 2011) is very similar to the setting of Carlin-type gold deposits in northern Nevada (Cline et al., 2005; Muntean et al., 2011). The deposits in both Guizhou and Nevada occur along deformed and rifted cratonic margins, marked by passive margin sequences containing significant amounts of carbonate rocks. The cratonic margins in Guizhou and Nevada were both deformed by later orogenies. The deposits in both localities are commonly hosted in compressional structures in carbonate rocks adjacent to high-angle faults.

In Nevada, Neoproterozoic rifting of western North America and opening of the Pacific Ocean led to clastic rift sediments overlain by a Cambrian-Devonian passive margin sequence dominated by carbonaceous carbonate rocks on the shelf and along the slope, with deep water siliciclastic and mafic volcanic rocks to the west. In Guizhou, Devonian rifting of the southwestern margin of the Precambrian Yangtze craton, related to formation of the Paleo-Tethys ocean, led to deposition of a thick sequence of Devonian to Triassic carbonate and siliciclastic rocks in the Youjiang Basin. Both passive margin sequences show evidence for syn-sedimentary faulting. In Nevada, the syn-sedimentary faulting is commonly manifested by carbonate debris flow breccias that preferentially host gold ore (Emsbo et al., 2006; Muntean et al., 2007). In Guizhou, sedimentation in the Youjiang Basin was controlled by a series of syn-sedimentary faults, where shallow water, fossiliferous limestones were deposited on submarine horsts; deep-water sediments, predominantly siliciclastic rocks as well as micrite and basalts, occur in the grabens.

Both passive margin sequences were then deformed. In Nevada, a series of orogenies beginning in the Late Devonian continued through the Mesozoic. The first, the Antler Orogeny, placed siliciclastic rocks over carbonate slope rocks along a regional thrust fault called the Roberts Mountains Thrust. Many of the very large Carlin-type deposits in Nevada are in the lower plate carbonates within a few hundred meters of this thrust, or its projection. Beginning in the Middle Triassic, the Youjiang Basin was inverted and developed into a foreland fold and thrust belt setting. However, unlike Nevada, Guizhou lacks the regional thrust faults that placed non-reactive siliciclastic rocks over reactive carbonate rocks. The shallow-water carbonate rocks in the horst blocks were gently folded whereas the deep basin rocks were tightly folded and thrusted. Classic inversion structures occur along the basin margins, such as at the Jingfeng deposit, where deep-water Triassic turbidites, mudstones, and argillaceous limestones were folded and thrusted westward against a basin-bounding high-angle normal fault that was reactivated as a reverse fault (Ilchik et al., 2005; Chen et al., 2011). This fault and other reverse faults in the basin show hanging wall anticlines and short-cut thrusts in their footwalls. The shallow water Permian limestones in the footwall of the basin-bounding fault are only broadly folded. Similar inversion structures have been documented in Nevada (Muntean et al., 2007).

Thus, Guizhou and Nevada share very similar geologic settings prior to Au mineralization. Deposits in both regions occur along rifted cratonic margins that have carbonate-bearing passive margin sequences. The carbonates, especially slope carbonates which are strongly carbonaceous, are more abundant in Nevada and host a larger proportion of the ore than in Guizhou. In both regions the original rift structures appear to have been continuously reactivated and to have localized subsequent deformation, first as syn-sedimentary faults and then inverted as reverse faults during orogenies. Many of the deposits occur near these deep structures. Examples of old reactivated structures likely linked to underlying lithospheric scale rift structures in Nevada include the Post, Cortez, and Getchell faults (Muntean et al., 2007). Similar regional structural zones in Guizhou include the Puding − Ceyang and Nanpanjiang fracture zones. These comparable geologic settings resulted in similar ore controls for the Carlin-type deposits in Nevada and Guizhou. Deposits in both regions are replacement bodies, though Guizhou deposits contain open-space-filling vein minerals, and either discordant bodies along high-angle faults and/or stratiform bodies along fa-

vorable carbonate-bearing units. Ore is commonly hosted by compressive structures such as folds and thrust faults. As pointed out above, many deposits in Nevada are also controlled by regional thrust faults that placed non-reactive siliciclastic rocks over reactive carbonate rocks. Nevertheless, in both regions deposits occur near structural culminations of highly fractured rocks, commonly with significant carbonate contents, above and near high-angle faults that were likely linked to underlying basement rift structures.

A key difference between the two regions is the presence of felsic magmatism in Nevada, both pre-ore granitic plutons and syn-ore Eocene dikes and volcanic rocks (Ressel and Henry, 2006). Several Carlin-type deposits in Nevada have a strong spatial association with pre-ore Mesozoic granites where ore is commonly localized along the fractured margins of the metamorphic contact aureole of these plutons where there exist strong contrasts in reactivity and rheology. The syn-ore Eocene dikes, which range from basalt to more commonly rhyolite in composition, locally contain ore, but commonly are weakly mineralized and were emplaced during the latest stages of hydrothermal activity. In contrast, except for pre-ore Late Paleozoic basalts within the Youjiang Basin, igneous rocks in Guizhou are limited to 85－89 Ma alkaline ultramafic dikes that appear to be spatially associated with the Puding－Ceyang fracture zone (Liu et al., 2010). Though volumetrically minor on the surface, magnetic and gravitational anomalies suggest more voluminous intrusions of these ultramafic rocks underlie southwest Guizhou (Zhang et al., 2003).

4.2. *Deposit geology*

4.2.1. Au-and As-rich sulfide minerals

The Au-and trace element-rich pyrites and marcasites found in Nevada Carlin-type deposits typically occur as rims on previously formed pyrites or as individual, anhedral, somewhat spherical clusters of pyrite or marcasite crystals in which non-ore cores are not apparent (Figs. 9a, 9b) (Wells and Mullins, 1973; Arehart et al., 1993; Cline, 2001). Where present, the non-ore cores vary from euhedral to anhedral and formed during earlier geologic events including diagenesis or hydrothermal activity related to older intrusions. Both the trace element-rich rims and spherical ore pyrites exhibit low relief, are somewhat darker in color and less reflective than typical pyrite, and have irregular, feathery outer edges, earning them the name "fuzzy" pyrites. Both the rims and spherical pyrites, when >2 to 3 μm in diameter, can be recognized under the microscope by relief, color, and texture. Their trace element-rich character is confirmed by either qualitative energy dispersive analyses (EDS) using the SEM that identify As, or electron probe microanalyses that commonly detect Cu, Hg, Tl, and Sb in addition to Au, in concentrations exceeding a few to several hundred parts per million (Longo et al., 2009; Muntean et al., 2011). Au concentrations in pyrite and marcasite range from detection limits (~170 ppm) to as much as 8 000 ppm; As commonly ranges from 5 to 15 wt%. Though the pyrites are not generally readily distinguished with a hand lens, they impart a "sooty" color to the rock when sufficiently abundant, and have also come to be referred to as "sooty" pyrites.

The readily identifiable low relief, sooty, poorly polished pyrite rims that characterize Nevada ore are not present in Guizhou. Instead, somewhat uncommon coarse pyrites have Au-and As-free cores and high relief, bright and brassy rims not visible under a microscope, but visible with BEI (Su et al., 2008; 2011). The coarse pyrite cores may have formed from geologic processes active prior to the ore-stage event. Alternatively, many fine-grained pyrites do not have rims visible either under the microscope or under BEI. These pyrites appear to contain increasing As + Au and other trace metals from the center of the crystal to the rim, rather than having discrete rims. Some of these fine-grained ore-stage pyrites were overgrown by arsenopyrite with lesser Au, suggesting increasing As and, initially increasing, then decreasing Au in the ore fluid as the pyrites and arsenopyrites formed. Examination of sample transects also shows a significant increase in pyrite in the rock with increasing grade, supporting nucleation and growth of most fine-grained pyrites during the ore stage as opposed to formation of fine-grained pyrite cores and rims during two separate hydrothermal events.

4.2.2. Sulfidation

A key characteristic of mineralization in Nevada CTGD is that the sulfide ore precipitated in response to sulfidation of host rock Fe (Hofstra et al., 1991; Stenger et al., 1998). Evidence for an early, Paleozoic Sedex or Mississippi Valley-type event in Nevada that fixed Fe in carbonate rocks has been identified at the Meikle (Emsbo, 1999; Evans, 2000; Emsbo et al., 2003) and Jerritt Canyon (Patterson, 2009) deposits. Subsequently, during the Eocene, ore fluids sulfidized Fe in the host rocks to form Au-bearing and trace element rich pyrite.

Preliminary studies reported here suggest that in the examined Guizhou deposits, Fe was added to calcite-rich sedimentary rocks now hosting the ore, altering calcite and/or dolomite to ferroan dolomite. Subsequently, ore fluids sulfidized this Fe forming ore-stage pyrite, and ferroan dolomite altered to dolomite. These observations are consistent with geochemical analyses that show an increase in Fe from least altered to weak or moderately altered rock, but which show no or minimal addition of Fe as high-grade rock formed, even though it contains significantly more ore pyrite. What is not clear is the timing of the introduction of Fe. Fe and S introduction during the ore event would constitute pyritization, whereas Fe metasomatism during an earlier geologic event followed by sulfidation during the hydrothermal Au event would be equivalent to the sulfidation process that formed the Nevada deposits. Careful paragenetic studies to identify the timing of the Fe metasomatism, accompanied by plots of Fe versus S in low-and high-grade rock to identify trends of either sulfidation or pyritization (Stenger et al., 1998; Cassinerio and Muntean, 2010), are needed to determine the process active in the Guizhou deposits. The marcasite-chalcopyrite-sphalerite mineralization identified in unaltered and weakly altered rocks in the Guizhou deposits might be evidence of an earlier hydrothermal event responsible for Fe metasomatism.

A somewhat related observation in the Guizhou deposits is the spatial association of pyrite with pyrobitumen, which suggests a link between Au mineralization and petroleum migration, as proposed by Gu et al., (2012). The Carlin deposits in Nevada also contain pyrobitumen and a general spatial relationship between it and Au during the early discovery and exploration of the Nevada deposits was observed. Subsequent studies (Kuehn and Rose, 1992; Emsbo et al., 2003) determined that in the Carlin trend, C in the host rocks was converted to pyrobitumen prior to ore deposit formation during the Eocene; however, a potential genetic link between Au and petroleum and/or bitumen in these deposits remains an open question to some researchers.

4.2.3. Alteration

Alteration processes in the Nevada deposits that accompanied sulfidation and formation of Au-bearing sulfides include decarbonatization, silicification, and argillization (Kuehn and Rose, 1992; Hofstra and Cline, 2000; Cline et al., 2005). The dominant and most consistent alteration feature in these deposits is decarbonatization, or the removal of CO_2 from carbonate minerals as they became unstable during hydrothermal ore deposition. Alteration produced a characteristic punky and porous texture in drill core (Fig. 5a) and, where intense, produced broken and rubbly fragments of very low-density rock. Decarbonatization was commonly accompanied by precipitation of quartz, which replaced carbonate minerals to form jasperoid (Fig. 5b). The quartz crystals generally contain encapsulated tiny crystals of carbonate minerals, confirming carbonate replacement (Cline, 2001). Small vugs in the rock, resulting from brecciation or decarbonatization, are locally rimmed by euhedral, drusy quartz crystals (Fig. 5c), and jasperoid and drusy quartz characterize these deposits, whereas veins do not and are typically not present. Clay minerals include illite, kaolinite, and/or dickite that replaced silicate components in the rocks (Fig. 5d), and which are consistent with low temperature alteration and mineralization and the acidic character of the ore fluid (Cline et al., 2005).

Alteration in the examined Guizhou deposits displays important differences from the Nevada deposits. Decarbonatization, which is the major alteration feature in Nevada, is not important, as Au-bearing pyrite is associated with dolomite and ferroan dolomite in addition to jasperoid and illite. In progressively altered rocks, calcite and sparry dolomite appear to have altered to ferroan dolomite that in high-grade rocks is replaced by dolomite. Drill core is typically unbroken and intact and the rock retains its original textures (Ilchik et al., 2005), though rock density was somewhat reduced. Geochemical data (Table 1) are consistent with partial decarbonatization as Ca is reduced by about half in altered samples, and Mg is reduced by half in the Shuiyindong transect and by about a third in the Zimudang transect.

The stable carbonate minerals in the Guizhou deposits examined in this study suggest that ore fluids were less acidic than the Nevada ore fluids, which is consistent with illite being the dominant clay and the rare occurrence of kaolinite, which is a common alteration mineral in the Nevada deposits. Collectively the observed alteration assemblages suggest a possibly higher temperature ore fluid than at Carlin in which there is less dissociation of carbonic acid, yielding a near-neutral and cooling ore fluid, quite different from the acidic Nevada ore fluid that routinely removed carbonate and produced kaolinite and marcasite.

4.2.4. Quartz

The occurrences of quartz suggest different geologic processes active during mineral precipitation in the two regions. Quartz in the Nevada deposits primarily replaced significant quantities of carbonate minerals. Lesser late-ore drusy quartz rims vugs, and vein quartz is notably absent (Lubben et al., 2012). In contrast, vein quartz is prominent in some Guizhou deposits (Su et al., 2009), and though replacement of carbonate minerals is important in some deposits and at least locally in others, particularly during the main-ore stage, the presence of calcite in ore suggests that jasperoid replacement was not as dominant a process in Guizhou as in Nevada. Though jasperoid replacement of carbonate at Guizhou could have resulted from fluid-rock reaction and decarbonatization, replacement may also have resulted from decreasing temperature as in epithermal deposits.

Another significant difference is the abundance of vein quartz in some Guizhou deposits, as quartz veins are rare in Nevada deposits. This absence of quartz veins indicates the importance of fluid-rock reaction and the presence of "passive and opportunistic" ore fluids that were underpressured, and only rarely created open space contemporaneous with mineralization. The abundant vein quartz at Guizhou indicates that, alternatively, these hydrothermal systems were more energetic and capable of creating significant open space. Angular wall rock fragments formed and spalled into fissure veins indicating pressure fluctuations in which overpressured fluids fractured the rock during pressure release. Jasperoid that replaced large volumes of carbonate rock indicates the overwhelming importance of fluid-rock reaction in the Nevada deposits; vein quartz that precipitated in open space at Guizhou, alternatively, indicates the importance of fluid cooling, possibly as a result of fluid immiscibility.

4.2.5. Late-ore stage minerals

Late ore-stage minerals in the Nevada deposits include primarily realgar, calcite, drusy quartz, orpiment, pyrite and/or marcasite, and less abundant to rare fluorite, stibnite, and cinnabar. Overgrowth relationships show a typical paragenetic sequence from early to late of orpiment + quartz, realgar, and calcite, which is consistent with declining formation temperatures from fluid inclusions (Hofstra and Cline, 2000; Cline, 2001). The sequence of formation of these minerals, their abundance in high-level structures, and geochemical modeling indicating precipitation in response to cooling (Hofstra et al., 1991) are consistent with their formation during collapse of the hydrothermal system. Realgar is the most readily identified mineral that typifies late-ore mineralization, and some deposits such as Getchell have abundant realgar in the upper levels of the main structure, the Getchell fault. However, at other deposits such as Betze-Post, realgar is present, but not abundant.

Late ore-stage minerals in the Guizhou deposits are similar to Nevada deposits, with the significant difference being the abundance of open-space-filling vein quartz. Another difference is the common precipitation of realgar after calcite in Guizhou deposits, while the general sequence is realgar followed by later calcite in Nevada deposits, though realgar does conform to euhedral calcite in some systems.

4.2.6. Fluid inclusion studies

Fluid inclusion studies from a number of deposits were summarized (Hofstra and Cline, 2000) to provide information about ore-stage and late ore-stage conditions in the Nevada deposits. The studies show that the deposits formed from low temperature aqueous fluids with low salinities and low volatile contents (Cline, 2001; Lubben et al., 2012). Fluid immiscibility did not occur and ore-stage minerals precipitated in response to fluid-rock reaction, whereas late ore-stage minerals precipitated as meteoric waters mixed with and diluted and cooled the ore-stage hydrothermal fluids.

Fluid inclusions in ore-stage jasperoid are consistently two-phase, liquid-rich inclusions, typically $\leqslant 5$ μm in diameter, and most homogenize between ~160 and 220 ℃ (Cline and Hofstra, 2000). CO_2 is not visible in the inclusions or detected by CO_2 ice melting or the presence of clathrate, though quadrupole mass spectrometer analyses of bulk inclusion fluids indicate $\leqslant$ ~2 to 4 wt% CO_2, and lesser concentrations of other vola-

tiles including CH_4, N_2, and H_2S. Ore fluid salinities are between 3 and 6 wt% NaCl equivalent (Hofstra and Cline, 2000). A correction for inclusion formation at depths of approximately 2 km, based on geologic reconstructions, apatite fission track studies and fluid inclusion characteristics, indicates trapping temperatures were about 180 to 240 ℃. Fluid inclusion studies of late ore-stage minerals indicate fluid temperatures declined to ~100 ℃ during precipitation of calcite, which filled significant open space and was the latest hydrothermal mineral to precipitate. Most late-ore calcite has salinities from 3 to 5 wt% NaCl equivalent. Late ore-stage CO_2 was not detected (Cline and Hofstra, 2000).

Fluid inclusion studies reported for the Guizhou deposits indicate fluid pressure, temperature, and chemistry were quite different in these deposits (Hu et al., 2002; Zhang et al., 2003; Su et al., 2009). In contrast to Nevada deposits, fluid inclusions in Guizhou deposits became increasingly CO_2-rich and were immiscible during the main-ore and late-ore stages. The fluids were also trapped under higher pressures at greater depths, and probably higher temperatures, than ore fluids in the Nevada deposits (Hu et al., 2002; Su et al., 2009). Using depths determined for main ore-stage mineralization (Su et al., 2009), we here apply a pressure correction to the pre main-ore inclusions, which yields trapping temperatures of about 220 – 345 ℃ (Bodnar and Vityk, 1994). This temperature range is considerably higher than temperatures generally reported for the Guizhou deposits, in part because pressure corrections have not generally been applied. The higher end of this range is more consistent with the reported observation of negative quartz crystal inclusion shapes.

Main-stage ore fluids in Guizhou have been interpreted to have resulted from immiscibility (Su et al., 2009); thus there is no pressure correction to homogenization temperatures of 190 to 245 ℃. However, two immiscible fluids have apparently not been observed coexisting in fluid inclusion assemblages, and the fluid identified as representing the second immiscible member was trapped in late ore-stage rather than main ore-stage minerals. Thus, it is possible that the main ore-stage fluid did not form through immiscibility. If so, a pressure correction would yield trapping temperatures for these fluids similar to trapping temperatures determined above for the pre main-ore fluids, again, considerably higher than temperatures at which the Nevada Carlin ore formed. Main-ore fluids in the Guizhou deposits are also different from the Nevada ore fluids in composition as they contain abundant CO_2; these fluids evolved to be essentially CO_2-only fluids during the late-ore stage. The increasing abundance of CO_2 in ore fluids at Guizhou has been attributed to decarbonatization of the host rock by the ore fluid (Su et al., 2009). However, this explanation raises questions given that decarbonatization was a much more thorough and voluminous process in the Nevada deposits, and the CO_2 that evolved did not impact the composition of the ore fluids.

5. Discussion and Conclusions

5.1. *Deposit characteristics*

Though deposit architecture, tectonic setting, and host rocks for the Guizhou and Nevada deposits appear to be quite similar, the ore-stage minerals, and fluids and processes that produced the minerals and deposits, have important differences. In Nevada, fluid-rock reaction between a low pH fluid and highly reactive rock yielded low pressure-temperature replacement ore assemblages. In Guizhou, CO_2-bearing ore fluids at temperatures and pressures possibly as much as 100 ℃ and 500 bars greater than temperatures and pressures of ore fluids in the Nevada deposits, precipitated Au-bearing pyrite. These potentially immiscible fluids were sufficiently overpressured to fracture wall rocks and to create significant open space filled by vein quartz. The fluids carbonatized host rocks and formed both replacement and open-space-filling ore, indicating active geologic processes at the site of the ore deposition similar to those that formed orogenic Au systems. As Guizhou deposits display characteristics similar to both Carlin-type and orogenic systems, these deposits may have formed at depths and temperatures intermediate to typical depths and temperatures for Carlin-type and deeper orogenic deposits. Detailed petrographic and fluid inclusion studies of additional deposits in Guizhou are needed to clarify the timing of Fe metasomatism, confirm alteration processes coincident with Au deposition, and confirm the similarities and differences between the Guizhou and Nevada deposits.

5.2. *Tectonic and geologic setting*

Based mainly on ages of the syn-ore dikes and direct ages of mineralization by Rb-Sr dating of the ore mineral galkhaite, a consensus was reached a decade ago that Carlin-type deposits in Nevada formed in the Late Eocene. Resolving the age of Carlin-type deposits in Nevada has been critical to constraining the tectonic setting and models of ore formation. A long-lived, east-dipping subduction zone was established along western North America by the Middle Triassic. In the Late Cretaceous the subducting slab began to shallow, and by 65 Ma magmatism had ceased in Nevada. Rollback or delamination of the shallow-dipping slab renewed magmatism at ~45 Ma, which swept southwestward at a high angle to the continental margin. Formation of the Carlin-type deposits tracked this southwestern sweep of magmatism in time and space across Nevada. The rollback of the slab appears to have been the critical tectonic trigger that led to the formation of Carlin-type deposits in the Late Eocene (Muntean et al., 2011). Rollback caused the asthenosphere to impinge on strongly hydrated sub-continental lithospheric mantle, resulting in profuse magmatism and a change from compression to extension in Nevada. Not only did Carlin-type deposits form during the slab rollback in Nevada, but also large porphyry copper (e. g., Copper Canyon), porphyry molybdenum (e. g., Mount Hope), and volcanic-hosted, low-sulfidation epithermal gold deposits (e. g., Round Mountain).

Li and Li (2007) proposed a similar tectonic model for South China. By the mid-Permian an active margin with a northwest-dipping subduction zone was established off the southeastern coast of South China. This active margin resulted in a coastal orogeny that shed terrestrial sediments to inland South China, including the Youjiang Basin, which then had become a foreland basin. The orogen and associated synorogenic magmatism began to migrate northwestward toward the craton, due to the start of flat-slab subduction, as proposed by Li and Li, (2007). By Late Triassic, both the orogenic front and the foreland basin had propagated more than 500 km into South China. Post-orogenic magmatism started at 190 Ma and migrated southeastward back toward the coast in the Jurassic and Cretaceous as a result of slab foundering and rollback. The large Jurassic porphyry copper and Cretaceous tin-tungsten skarn/vein deposits of South China are related to this magmatism.

Whether or not the Carlin-type deposits in Guizhou are related to slab rollback is critically dependent on the age of the deposits. Similar to the Nevada deposits prior to 2000, little consensus exists on the age of the Carlin-type deposits in Guizhou. Published age data range from Late Permian to Cretaceous. Gu et al. (2012) recently summarized existing geochronological dating and concluded the age of the Jingfeng deposit was ~190 Ma, based on a Re-Os isochron age on arsenian pyrite and a $^{40}Ar/^{39}Ar$ plateau age on sericite from quartz-calcite veins interpreted to be coeval with Au mineralization. However, Re-Os ages on pyrite are problematic given the possibility of analyzing multiple generations of pyrite, both pre-ore and ore-stage, which commonly occurred in the Carlin-type deposits in Nevada. Mesozoic ages on sericite in ore samples from Nevada deposits were shown to be irrelevant, because the sericite was eventually demonstrated to be pre-ore. Su et al. (2009) obtained Sm-Nd ages of ~135 Ma on calcite veins on the periphery of the Shuiyindong deposit; however, whether or not the veins are clearly related to gold mineralization has not been established. Other techniques tried in Guizhou, such as Rb-Sr on fluid inclusions and fission track dating of quartz are problematic or not widely accepted. Therefore, much like the Carlin-type deposits in Nevada, careful studies need to be done to establish the paragenesis and isolate the minerals that are truly affected by Au mineralization, either minerals that formed during Au mineralization or minerals that had their geochronometers completely reset by the hydrothermal system associated with the Au mineralization. The deposits in Guizhou are clearly hosted in compressional structures; however, is the mineralization syn-compression or, like Nevada, are the compressional structures much older than the mineralization?

Acknowledgements

We would like to thank and acknowledge all of the individuals at the Shuiyindong, Zimudang, Taipingdong, Yata and Jinfeng deposits for access to the deposits and drill core for sampling, excellent mine tours, and wonderful hospitality during our visit. We would also like to acknowledge financial support from Key Project 40930423 from the National Natural Science Foundation of China.

References

Arehart G B, Chryssoulis S L, Kesler S E. 1993. Gold and arsenic in iron sulfides from sediment-hosted disseminated gold deposits: Implications for depositional processes. Economic Geology, 88: 171-185.

Ashley R P, Cunningham C G, Bostick N H, Dean W E, Chou I M. 1991. Geology and geochemistry of the sedimentary-rock-hosted disseminated gold deposits in Guizhou Province, People's Republic of China. Ore Geology Reviews, 6: 131-151.

Bodnar R J, Burnham C W, Sterner S M. 1985. Synthetic fluid inclusions in natural quartz, III, Determination of phase equilibrium properties in the system H_2O-NaCl to 1000 ℃ and 1500 bars. Geochimica et Cosmochimica Acta, 49: 1861-1873.

Bodnar R J, Vityk M O. 1994. Interpretation of microthermometric data for H_2O-NaCl fluid inclusions. De Vivo B, Frezzotti M L. Fluid Inclusions in Minerals, Methods and Applications. Blacksburg, VA: Virginia Tech: 117-130.

Cassinerio M D, Muntean J L. 2011. Patterns of lithology, structure, alteration and trace elements around high-grade ore zones at the Turquoise Ridge gold deposit, Getchell district, Nevada. Steininger R C, Pennell W M. Great Basin Evolution and Metallogeny. Geological Society of Nevada 2010 Symposium Proceedings. Reno, Nevada: 949-978.

Chen M H, Huang Q W, Hu Y, Chen Z Y, Zhang W. 2009. Genetic types of phyllosilicate (mica) and its ^{39}Ar-^{40}Ar dating in Lannigou gold deposit, Guizhou province, China. Acta Mineralogica Sinica, 29: 353-362 (in Chinese with English abstract).

Chen M H, Mao J W, Bierlein F P, Norman T, Uttley P J. 2011. Structural features and metallogenesis of the Carlin-type Jinfeng (Lannigou) gold deposit, Guizhou Province, China. Ore Geology Reviews, 43: 217-234.

Chen M H, Mao J W, Qu W J, Wu L L, Uttley P J, Norman T, Zheng J M, Qin Y Z. 2007. Re-Os dating of arsenian pyrites from the Lannigou gold deposit, Zhenfeng, Guizhou Province, and its geological significances. Geological Reviews, 53: 371-382 (in Chinese with English abstract).

Chen M H, Zhang W, Yang Z X, Lu G, Hou K J, Liu J H. 2009. Zircon SHRIMP U-Pb and Hf isotopic composition of the Baiceng ultrabasic rock dykes in Zhenfeng county, southwestern Guizhou Province, China. Mineral Deposits, 28(3): 240-250 (in Chinese with English abstract).

Cline J S, Hofstra A H, Muntean J L, Tosdal R M, Hickey K A. 2005. Carlin-type gold deposits in Nevada: Critical geologic characteristics and viable models. Economic Geology, 100th Anniversary Volume: 451-484.

Cline J S, Hofstra A H. 2000. Ore fluid evolution at the Getchell Carlin-type gold deposit, Nevada, USA. European Journal of Mineralogy, 12: 195-212.

Cline J S. 2001. Timing of gold and arsenic sulfide mineral deposition at the Getchell Carlin-type gold deposit, North-central Nevada. Economic Geology, 96: 75-90.

Cunningham C G, Ashley R P, Chou I M, Huang Z H, Wan C Y, Li W K. 1988. Newly discovered sedimentary rock-hosted disseminated gold deposits in the People's Republic of China. Economic Geology, 83: 462-469.

Cunningham C G, Austin G W, Naeser C W, Rye R O. 2004. Formation of a paleothermal anomaly and disseminated gold deposits associated with the Bingham Canyon porphyry Cu-Au-Mo system, Utah. Economic Geology, 99: 789-806.

Emsbo P, Groves D I, Hofstra A H, Bierlein F P. 2006. The giant Carlin gold province: A protracted interplay of orogenic, basinal, and hydrothermal processes above a lithospheric boundary. Mineralium Deposita, 41: 517-525.

Emsbo P, Hofstra A H, Lauha E A, Griffin G L, Hutchinson R W. 2003. Origin of high-grade gold ore, source of ore fluid components, and genesis of the Meikle and neighboring Carlin-type deposits, Northern Carlin trend, Nevada. Economic Geology, 98: 1069-1100.

Emsbo P, Hutchinson R W, Hofstra A H, Volk J A, Bettles K H, Baschuk G J, Johnson C A. 1999. Syngenetic Au on the Carlin trend: Implications for Carlin-type deposits. Geology, 27: 59-62.

Evans D C. 2000. Carbonate-hosted Breccias in the Meikle Mine, Nevada and Their Relationship with Gold Mineralization. Unpublished MS Thesis. Golden, Colorado: Colorado School of Mines: 1-266.

Gu X X, Zhang Y M, Li B H, Dong S Y, Xue C J, Fu S H. 2012. Hydrocarbon-and ore-bearing basinal fluids: A possible link between gold mineralization and hydrocarbon accumulation in the Youjiang basin, South China. Mineralium Deposita, 47: 663-682.

Guo Z C. 1988. A preliminary discussion on the geological characteristics and genesis of Zimudang gold deposit, Guizhou Province. Guizhou Geology, 5: 201-217 (in Chinese).

He M Y. 1996. Physicochemical conditions of differential mineralization of Au and As in gold deposits, southwest Guizhou Province, China. Chinese Journal of Geochemistry, (2): 189-192.

Henry C D. 2008. Ash-flow tuffs and paleovalleys in northeastern Nevada: Implications for Eocene paleogeography and extension in the Sevier hinterland, northern Great Basin. Geosphere, 4: 1-35.

Hofstra A H, Cline J S. 2000. Characteristics and models for Carlin-type gold deposits. Thompson T B. Society of Economic Geology

Reviews 13, Gold in 2000. Denver, CO: 163-220.

Hofstra A H, Snee L W, Rye R O, Folger H W, Phinisey J D, Loranger R J, Dahl A R, Naeser C W, Stein H J, Lewchuk M. 1999. Age constraints on Jerritt Canyon and other Carlin-type gold deposits in the western United States: Relationship to Mid-Tertiary extension and magmatism. Economic Geology, 1999, 94: 769-802.

Hu R Z, Su W C, Bi X W, Tu G C, Hofstra A H. 2002. Geology and geochemistry of Carlin-type gold deposits in China. Mineralium Deposita, 37: 378-392.

Ilchick R P, Uttley P J, Corben R, Zhang A Y M, Alex Y M, Ham A, Andrew, Hodkiewicz P. 2005. The Jinfeng gold deposit: Mining the new frontier of China. Rhoden H N, Steininger R C, Vikre P G. Geological Society of Nevada Symposium 2005: Window to the World. Reno, Nevada: 887-898.

Kuehn C A, Rose A R. 1992. Geology and geochemistry of wall-rock alteration at the Carlin gold deposit, Nevada. Economic Geology, 87: 1697-1721.

Li Z X, Li X H. 2007. Formation of the 1300-km-wide intracontinental orogen and postorogenic magmatic province in Mesozoic South China: A flat-slab subduction model. Geology, 35: 179-182.

Liu J Z. 2001. Geological characteristics of Yanshang Carlin-type gold deposit. Guizhou Geology, 18: 174-178 (in Chinese with English abstract).

Liu S, Su W, Hu R, Feng C, Gao S, Coulson M, Wang T, Feng G, Tao Y, Xia Y. 2010. Geochronological and geochemical constraints on the petrogenesis of alkaline ultramafic dykes from southwest Guizhou Province, SW China. Lithos, 114: 253-264.

Longo A A, Cline J S, Muntean J. 2009. Detecting ore fluid pathways in Carlin-type gold deposits using pyrite chemistry. Williams P J. Smart Science for Exploration and Mining. Society for Geology Applied to Mineral Deposits, Proceedings 1: 242-244.

Lubben J, Cline J S, Barker S. 2012. Silicification across the Betze-Post Carlin-type Au deposit: Clues to ore fluid properties and sources, northern Carlin trend, Nevada. Economic Geology, 107: 1351-1385.

Mao S H. 1991. Occurrence and distribution of invisible gold in a Carlin-type gold deposit in China. American Mineralogist, 76: 964-972.

Muntean J L, Coward M P, Tarnocai C A. 2007. Reactivated Palaeozoic normal faults: Controls on the formation of Carlin-type gold deposits in north-central Nevada. Reis A C, Butler R W H, Graham R H. Deformation of the Continental Crust: The Legacy of Mike Coward. Geological Society London, Special Publications 272: 573-589.

Muntean J L, Cline J S, Simon A, Longo A A. 2011. Origin of Carlin-type gold deposits. Nature Geoscience, 4: 122-127.

Patterson L M. 2009. Hydrothermal Footprint of the Carlin-type Gold Deposits at the District Scale: Jerritt Canyon Mining District, Elko County, Nevada. Unpublished MS Thesis. Reno, Nevada: University of Nevada Reno: 1-240.

Peters S G, Huang J Z, Li Z P, Jing C G. 2007. Sedimentary rock-hosted Au deposits of the Dian-Qian-Gui area, Guizhou, and Yunnan provinces, and Guangxi district, China. Ore Geology Reviews, 31: 170-204.

Reich M, Kesler S E, Utsunoyiya S, Palenik C S, Chryssoulis S, Ewing R C. 2005. Solubility of gold in arsenian pyrite. Geochemica et Cosmochimica Acta, 69: 2781-2796.

Ressel M W, Henry C D. 2006. Igneous geology of the Carlin trend, Nevada: Development of the Eocene plutonic complex and significance for Carlin-type gold deposits. Economic Geology, 101: 347-383.

Simon G, Kesler S E, Chryssoulis S. 1999. Geochemistry and textures of gold-bearing arsenian pyrite, Twin Creeks, Nevada: Implications for deposition of gold in Carlin-type deposits. Economic Geology, 94: 405-422.

Stenger D P, Kesler S E, Peltonen D R, Tapper C J. 1998. Deposition of gold in Carlin-type deposits: The role of sulfidation and decarbonation at Twin Creeks, Nevada. Economic Geology, 93: 201-215.

Su W C, Heinrich C A, Pettke T, Zhang X C, Hu R Z, Xia B. 2009a. Sediment-hosted gold deposits in Guizhou, China: Products of wall-rock sulfidation by deep crustal fluids. Economic Geology, 104: 73-93.

Su W C, Hu R Z, Xia S, Xia Y, Liu Y P. 2009b. Calcite Sm-Nd isochron age of the Shuiyindong Carlin-type gold deposit, Guizhou, China. Chemical Geology, 258: 269-274.

Su W C, Xia B, Zhang H T, Zhang X C, Hu R Z. 2008. Visible gold in arsenian pyrite at the Shuiyindong Carlin-type gold deposit, Guizhou, China: Implications for the environment and processes of ore formation. Ore Geology Reviews, 33: 667-679.

Su W, Zhang H, Hu R, Ge X, Xia B, Chen Y, Zhu C. 2011. Mineralogy and geochemistry of gold-bearing arsenian pyrite from the Shuiyindong Carlin-type dold deposit, Guizhou, China: Implications for gold depositional processes. Mineralium Deposita, Doi: 10.1007/s00126-0328-9.

Su W C. 2002. The Hydrothermal Fluid Geochemistry of the Carlin-type Gold Deposits in Southwestern Yangtze Craton China. Unpublished PhD thesis. Guiyang, China: Institute of Geochemistry, Chinese Academy of Sciences (in Chinese with English abstract).

Tao C G, Liu J S, Dan G. 1987. On the gold ore deposit geological characteristics and genesis of Yata, Ceheng. Guizhou Geology, 4: 135-150 (in Chinese).

Tretbar D, Arehart G B, Christensen J N. 2000. Dating gold deposition in a Carlin-type gold deposit using Rb/Sr methods on the mineral galkhaite. Geology, 28: 947-950.

Wang Y G, Suo S T, Zhang M F. 1994. Tectonics and Carlin-type Gold Deposits in Southwestern Guizhou. Beijing: Geological Publishing House: 1-115 (in Chinese).

Wells J D, Mullins T E. 1973. Gold-bearing arsenian pyrite determined by microprobe analysis, Cortez and Carlin gold mines, Nevada. Economic Geology, 68: 187-201.

Xia Y. 2005. Characteristics and Model for Shuiyiodong Gold Deposit in Southwestern Guizhou, China. Unpublished PhD thesis. Guiyang, China: Institute of Geochemistry, Chinese Academy of Sciences (in Chinese with English abstract).

Ye X X, Wan G Q, Sun Z Y, Liu Y K, Zhou L D, Liu S R, Xue D J, Rivers L, Jones K W. 1994. Microbeam analysis of gold in Carlin-type gold deposits, southwestern Guizhou. Science in China: Series B, 24: 883-889 (in Chinese).

Zaw K, Peters S G, Paul C P, Burrett C, Hou Z. 2007. Nature, diversity of deposit types and metallogenic relations of South China. Ore Geology Reviews, 31: 3-47.

Zhang X C, Spiro B, Halls C, Stanley C J, Yang K Y. 2003. Sediment-hosted disseminated gold deposits in Southwest Guizhou, PRC: Their geological setting and origin in relation to mineralogical, fluid inclusion and stable-isotope characteristics. International Geology Review, 45: 407-470.